Republic of Iraq
Ministry of Higher Education and Scientific Research
University of Babylon
College of Education for Pure Sciences
Department of Physics

Study of the Core-Polarization Effects Using Microscopic Shell Model Calculations for Some Nuclei

A Thesis

Submitted to the Council of College of Education for Pure Sciences,

University of Babylon in Partial Fulfillment of the Requirements for the Degree of Master in Education/Physics

By

Sajad Ali Khashan Madi

(B.Sc. in physics, University of Babylon, 2018)

Supervised by

Prof. Dr.Khalid S. Jassim

2023 A.D. **1445 A.H.**

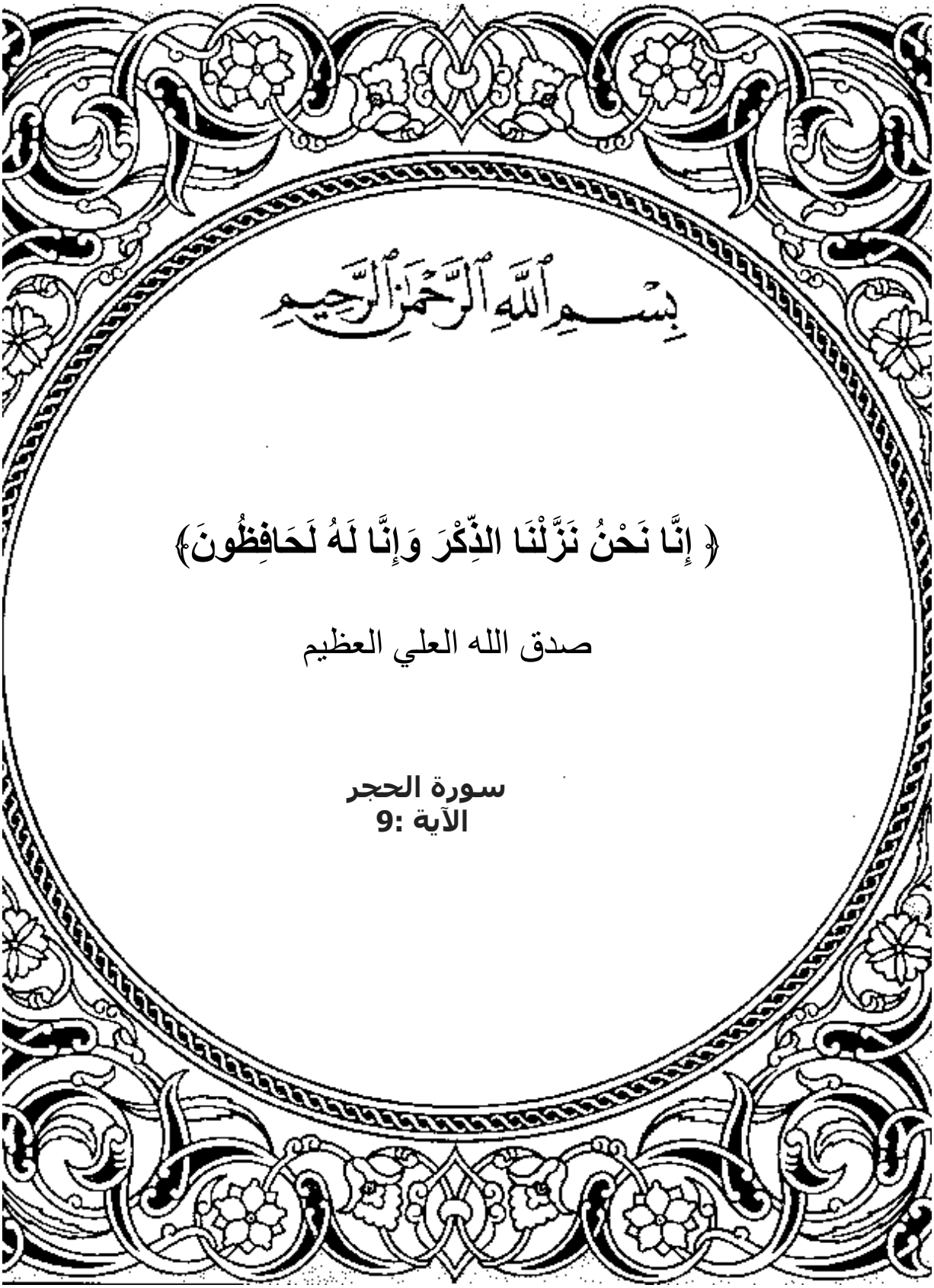
بِسْمِ اللَّهِ الرَّحْمَنِ الرَّحِيمِ
﴿ إِنَّا نَحْنُ نَزَّلْنَا الذِّكْرَ وَإِنَّا لَهُ لَحَافِظُونَ﴾
صدق الله العلي العظيم
سورة الحجر
الآية :9

Supervisor's Certificate

I certify that this thesis, entitled (**Study of the Core-Polarization Effects Using Microscopics Shell Model Calculations for Some Nuclei)** was prepared by the student (**Sajad Ali Khashan Madi)** under my supervision at the College of Education for pure sciences, University of Babylon in partial fulfillment of the requirements for the Degree of Master in Education / Physics.

Signature:
Name: Dr. Khalid S. Jassim
Title: Professor
(Supervisor)
Date: / /2023

Head of the Department Certificate

In view of the available recommendation, I forward this thesis for debate by the examining committee.

Signature:
Name: Dr. Khalid H. Abbas
Title: Professor
(Head of Physics Department)
Date: / / 2023

Examining Committee Certification

We certify that we have read the thesis entitled **"Study of the Core-Polarization Effects Using Microscopic Shell Model Calculations for Some Nuclei "** by "**Sajad Ali Khashan Madi** " and as a committee examined the student in its contents and, according to our opinion, it is accepted as a thesis for the degree of Master in Education / Physics.

Signature:

Name: Dr. Fadhil I. Sharrad

Title: Prof.

Address: University of Alkafeel

Date: / / 2023

Chairman

Signature:

Name: Dr. Salar H. Ibrahem

Title: Assist.Prof.

Address: University of Babylon

Date: / / 2023

Member

Signature:

Name: Dr. Fatima M . Hussien

Title: Assist.Prof.

Address: University of Babylon

Date: / / 2023

Member

Signature:

Name: Dr. .Khalid S. Jassim

Title: Prof.

Address: University of Babylon

Date: / / 2023

Member / Advisor

I hereby certify the decision of the examining committee.

Signature:

Name: Bahaa Hussein Salih Rabee

Title: Professor

Address: Dean of the College of Education for Pure Science**,** University of Babylon

Date: / / 2023

Scientific Supervisor Certification

This is to certify that I have read this thesis entitled **" Study of the Core-Polarization Effects Using Microscopics Shell Model Calculations for Some Nuclei "** and I found that this thesis is qualified for debate.

Signature:

Name: Dr. Murtadha Shakir Aswood

Title: Professor

Address: University of AL-Qadisiyah
Date: / /2023

Scientific Supervisor Certification

This is to certify that I have read this thesis entitled **“ Study of the Core-Polarization Effects Using Microscopics Shell Model Calculations for Some Nuclei ”** and I found that this thesis is qualified for debate.

Signature:

Name: Dr. Samah Oudah Hassoon

Title: Assistant professor

Address: University of Kufa

Date: / /2023

Scientific Supervisor Certification

This is to certify that I have read this thesis entitled **“ Study of the Core-Polarization Effects Using Microscopics Shell Model Calculations for Some Nuclei ”** and I found that this thesis is qualified for debate.

Signature:

Name: Dr. Ahmed Rawdhan Salman

Title: Assistant professor

Address: Al-Mustaqbal University

Date: / /2023

Dedication

To my father who brought me to this place, may God have mercy on him soul.

My Lord prolong my mother's life and keep her for me.

To all my supportive friends.

sajad

Acknowledgments

First of all, Praise is to Allah, Mercy and peace are to the Prophet Mohammed and his relatives and companions.

I would like to sincerely thank my supervisor **Prof. Dr. Khalid Salih Jasim** for his direction, assistance, guidance, and his recommendations and suggestions for this work.

I am deeply indebted to the head of the Department of Physics, the staff and the dean of the College of Education for Pure Sciences for the support that provided.

I wish to express my thanks to all my friends, especially the master group for their kind assistance and support during our course study and thesis work.

sajad

Abstract

The electron scattering transverse form factors for some selected states of ^{51}V,^{59}Co,^{93}Nb, and ^{115}In nuclei with electron scattering longitudinal form factors for some selected states of $^{42,44,48}Ca$, $^{58,60,62}Ni$ nuclei lie in the fp-shell region have been investigated. The shell model calculations have been performed using the recent version of the shell model code NushellX@MSU.

The effective interactions employed for nuclei to calculate the eigenvalue and eigenvectors that are used to calculate the one body transition densities (OBTD) to be used in the calculations of the inelastic electron scattering form factors.

Tassie and Bohr-Mottelson models are employed to calculate the inelastic electron scattering form factors with harmonic oscillator (HO) as residual effective interaction.The proton and neutron effective charges are used to account for the core polarization effects.

The Skyrme effective interaction with (Sk35)parametrization was used in the calculation of the form factors using the model space wave function generated from the overlapping of all the wavefunctions resulted from configuration mixing of all the states of the adopted model space with and without restrictions imposed on the model space. The calculated inelastic electron scattering form factors for the studied nuclei were compared with the available experimental data. The effect of core polarization by means of effective proton and neutron charges is found very essential to be considered that improves the agreement with the experimental data very well, especially for the Coulomb C2 and C4 form factors. The magnetic form factors are less or not affected by the change of the effective proton and neutron charges.

Contents

List of Figures

list of symbols and abbreviations

Symbol or Abbreviation	Meaning
OBTD	One body transition densities
SP	single-particle
NN	nucleon-nucleon
F^{co}	Longitudinal or Coulomb form factor
F^{T}	transverse form factor
$J(T)$	current density
M1, E2	Magnetic and electric multi-poles
TBME	Two body matrix element
BM	Bohr-Mottelson model
Vm	Valence model
TM	Tassie Model
$H^{(0)}$	unperturbed Hamiltonian
T_i	Kinetic energy
$U_{(i)}$	potential energy
NuShellX@MSU	Shell model code by B. Rae and B. A. Brown
$\hbar$	Planck constant reducer
ψ	Wave function
k	Electron wave number
λ	Wavelength
PWBA	Plane Wave Born approximation
DWBA	Distributed Wave Born approximation
Ze	Charge of nucleus
c	Speed of light
M3Y	Michigan three range Yukawa
$\frac{d\sigma}{d\Omega}$	Differential cross section for the scattering
CDD	charge density difference
σ_M	Mott cross section
α	Fine structure constant
E_i	Energy of incident electron
f_{rec}	The recoil factor of the nucleus
ω	The energy transfer
q	Three momentum transfer
q_μ	Four-momentum transfer
$F_J^{\eta}(q)$	(Longitudinal and Transverse) form factor
J	Total angular momentum

T	Total isospin
T_z	Projection isospin
m_o	The rest mass of the electron
$n!$	Factorial of n
$n!!$	Double Factorial of n
$\Phi^{core}_{J,\tau}$	Wavefunction for core
φ_{a1}	The single-particle wavefunctions
b	Size parameter for HO
L	Orbital angular momentum quantum number
OBDM	One-body density matrix
$\left\{ \begin{matrix} .... \\ .... \\ .... \end{matrix} \right\}$	9j-symbols
$\left(\begin{matrix} .... \\ .... \end{matrix} \right)$	3j-symbols
$\hat{\rho}(\vec{r}, t_z)$	Nucleon charge density operator
$\hat{T}_{J,t_z}$	The longitudinal operator
$j_J(qr)$	Spherical Bessel function
$Y_{JM}(\Omega)_r$	Spherical harmonic function
$\delta(\vec{r} - \vec{r}_i)$	Dirac delta function
$F_{c.m}(q)$	Center of mass form factor
$F_{f.s}(q)$	Form factor due to the nucleon-finite size
$d\Omega$	Solid angle
Ω	Angular frequency
H	Hamiltonian
A	Mass number of nucleus
Z	Atomic number of the nucleus
CP	Core polarization
USDA	Universal sd-shell interaction A
MS	Model space
Γ	Gamma function
$F(a; b; y)$	The confluent hyper-geometric function
ρ_{Jt_z}	The transition charge density
q_{eff}	Effective momentum transfer
(rms)	The root mean square
B(CJ)	Reduced transition probability
$R_{nl}(r)$	Radial part of the single-particle wave function
C2,C4	Longitudinal Coulomb form factor for J=2 and J=4

SKx	SKyrme-Hartree Fock potential
HO	Harmonic oscillator
WS	Wood-Saxon
∇^2	Laplace operator
B(WL)	reduced transition probabilities
FB	Fourier-Bessel expansion
SOG	Sum of Gaussians expansion

CHAPTER ONE

GENERAL INTRODUCTION

1.1 Introduction

The aim of nuclear physics is to understand the nuclear structure and the nature of interactions between nucleons, which are strong interactions that have a significant impact on determining the characteristics of nuclei[1].For simulations of nuclear structure using nucleons, the shell model serves as the fundamental framework. More than fifty years ago, when this concept first appeared in nuclear physics,[2, 3].The shell model is considered of as one of the most significant nuclear models utilized to comprehend the fundamental characteristics of the structure According to the nuclear model, the nucleus is made up of nucleons that are placed in certain shells, much like how electrons are grouped in atomic shells. Each nucleon moves independently of the others, but they all move in the nuclear field (potential) that is created by all of them[4]. Nuclear shell model calculations are a key theoretical tool for studying nuclei characteristics. It may be employed in its most basic single-particle version to provide a qualitative insight, but it can also serve as the foundation for far more complicated and comprehensive computations[5].The shell model has a significant position due to the fact that it is a more fundamental framework with fewer assumptions and that it has been incredibly successful in representing the nuclei at low excitation energies[6].

The first step in any shell-model computation is to define the "model space," or the collection of active single-particle (SP) orbits. The Hamiltonian matrix must be built up and diagonalized in this condensed Hilbert space. The residual contact between valence nucleons is a fundamental input, as was previously indicated. In actuality, this is a "model-space effective interaction," which varies in a number of ways from the contact between free nucleons. In reality, it must take into account the configurations omitted from the model space in addition to being residual in the sense indicated above. Unsurprisingly, one of the main objectives of nuclear physics is to comprehend the characteristics of nuclei by beginning with the interactions between nucleons. The nucleons in a nucleus are now thought of as non-relativistic particles that interact via a Hamiltonian made up of two-body, three-body, and higher body

potentials, with the nucleon-nucleon (NN) term being the dominating one[7].

Both quantum mechanics and the Pauli exclusion principle are compatible with the shell model. The nuclear shell model may be applied to a wide range of potentials, including the infinite dimension potential, the Harmoic oscillator (HO) potential, the Wood-Saxons (WS) potential, the Skyrme-Hartree (SKX) potential, and many more [8].

The nuclear structure may be well understood by the high-energy electron scattering from the nucleus[9].Form Factors make electron nucleus scattering a very effective tool for understanding the nuclear structure. As the contact between the electron and the target nucleus is quite mild, measurements may be made on the target nucleus without significantly altering its structure[10].In contrast, in the case of heavily interacting projectiles, it is difficult to distinguish between the structural effects on the target and the scattering process. Using electron scattering, it is simple to connect the cross section to the local charge and current density operators' transition matrix components and, consequently, to the target's actual structure.The use of photon excitation is another method for studying the nuclear structure via electromagnetic interaction. The three-momentum sent (q) to the nucleus can be changed for a given energy loss of the electron, but electrons have a significant advantage over other particles in that the four-momentum transferred (q_μ^2) in the scattering must have a space-like distribution. Nevertheless, compared to electron scattering, photon scattering has a significant disadvantage in that it cannot detect the ground state of the nucleus; instead, it can only detect excited states, with momentum transfer(q) equal to nuclear excitation energy [11].

Mott conducted the first investigation into electron scattering in 1929, when he estimated the cross section for such scattering from a point nucleus of charge called Ze[12].Using a factor that is dependent on the distributions of charge, current, and magnetization in the target nucleus, known as the nuclear form factor, the Mott's cross section may be multiplied to account for the nuclear size. The incident and

scattered electron energies as well as the scattering angle may be used to compute the form factor empirically as a function of the nucleus's momentum transfer(q), There are two ways that the target nucleus's electrons might scatter:
The first is, if the scattered electron's energy does not change and it leaves the nucleus in its ground state after scattering. It is known as elastic scattering.
The second is, if the electron is in an excited state when it leaves the nucleus and scatters with a final energy that is less than its beginning energy by a portion of the energy that was transferred to the nucleus to be in the excited state. It is known as inelastic scattering[11].

Theoretically, the calculation of electron scattering cross section, multipole form factor, multipole transition probability, binding energies, separation energies, displacement energies, intruder states, proton and neutron halos, diproton decay, spectroscopic factors, interaction cross sections, E1 and E2 transitions, beta decay, quadrupole moments and magnetic moments....etc need the modification of theoritical model, computer ability and computer programes so that different theoretical models have been suggested in order to make a best theoretical framework for these nuclear properties calculation and the nuclear shell model is one of the most important model used to calculate the properties of nuclei and nuclear phenomena and the nuclear shell model codes like OXBASH[13], MSHELL[14], ANTOINE[5], RETSSCHIL[15], VECSSE[16],NATHAN[17], and NuShellX@MSU[18].are widly used. In addition to the single particle wave function, the two-body matrix element (TBME) plays a crucial role in the calculation of the aforementioned nuclear properties, leading to the suggestion of various shell model spaces for effective interactions based on the strength of the two-body interactions, a variable obtained from actual nuclear interactions, and the fitting process[19].

Important knowledge and data on the nucleus are obtained as a result of the high-energy electron scattering. The amount of information gained from high energy electron scattering by nuclei depends on the electron's associated de Broglie wavelength's magnitude in relation to

the variety of nuclear forces. The de Broglie wavelength corresponds to the nucleus spatial expansion when the energy of the entering electron is 100 MeV or higher. The electron is thus a perfect probe for studying nuclear structures with this energy[9].

Both the longitudinal (Coulomb) form factor (F^{co}), which is the Fourier transform of the charge density $\rho(r)$, and the transverse form factor (F^{T}), which is the Fourier transform of the current density $J(T)$, are components of the form factor. Electric (E) and magnetic (M) transverse form factors are distinguished (M). Only electric multipoles can have longitudinal components, but both electric and magnetic multipoles can have transverse components, according to the parity and angular momentum selection rules[11, 20].

Theoretical computation of the electron scattering cross section for different form factors, multi-pole transition probability, etc. electron scattering may be used to find all of them. In order to calculate the wave functions for the nuclear shell model, wave functions derived from Schrodinger's differential equation, such as the HO potential energy functions, WS potential, and SKX potential, are employed[21].

It is possible to account for Core-Polarization (CP) effects by specifying effective operators in the MS that may be calculated using perturbation theory. When it was initially discovered that there were differences between experimental values for nuclear magnetic moment, quadruple moments, gamma-transition rates, etc. and the predictions of the basic shell model, this hypothesis first surfaced in the literature around a century ago[22]. Several attempts were made to find reasonable model for the calculation of the CP effects . Some of these attempts include the Bohr-Mottelson model(BM) [23], the Valence model(VM)[24], and the Tassie Model (TM)[25]. Moreover, some groups employed the first and second orders perturbation theory to explain the CP effec

1.2 Literature Survey

The following are some of the themes that are pertinent to the current study and have been widely explored in relation to (even-even) and(Odd-even or even-Odd) nucleus structure ,and one may evaluate these studies about the current work:

Jassim (2012) [26]. studied the longitudinal and transverse electron scattering form factors and transition probabilities for various states in the nuclei of ^{10}B, ^{32}S, and ^{48}Ca. A microscopic theory was used to account for the core-polarization (CP) effect, which is the result of high configuration occurring outside of the model space.

Jassim and Kassim (2013)[27].studied inelastic electron scattering form factors in several odd-A sd-shell nuclei ^{17}O,^{27}Al, and ^{39}K to account for higher energy combinations outside the sd-shell model universe. Utilizing the Wildenthal contact between two entities, the sd-shell describe space. Researchers have investigated the OBDM elements for the longitudinal C2 and C4 transition for the ^{27}Al nucleus, and the interaction between the CP matrix elements and first order perturbation theory is taken into consideration via the (M3Y) interaction. The form factor is drastically changed when CP effects are taken into account, and the experimental data can be accurately described in terms of both the absolute strength and the dependence on the q. Sd-shell model calculations are unable to adequately describe both the transition strength and the form factor.

Salman *et al.* (2013) [28]. studied the form factors for the inelastic electron scattering to $2^+, 4^+$ states in $^{46,48,50}Ti$, in the framework of shell model. The calculation is performed in $(0f_{7/2}, 1p_{3/2}, 0f_{5/2}, 1p_{1/2})$ model space as well as extended 6 model space.

Jassim *et al.*(2014)[29].studied that Nuclear structure (energy levels, elastic and inelastic electron-nucleus scattering, and transition probability) of ^{23}Na,^{25}Mg,^{27}Al, and ^{41}Ca nuclei have been studied using shell-model calculations. Set of two-body interactions are used in this

paper. The universal sd of the Wildenthal interaction in the proton-neutron formalism, universal sd-shell interaction A (USDA) universal sd-shell interaction B (USDB) and GXFP1 interaction for the fp-shell is used with the nucleon-nucleon realistic interaction Michigan three-range Yukawa (M3Y) as a two-body interaction for core-polarization calculations.

Jassim and Abdul-Hamza(2014)[30].studied some fp-shell nuclei. For the computations of the Core-Polarization effects for the atoms $^{42,44,48}Ca$, $^{46,48,50}Th$, and $^{50,52}Cr$, used the GXPF1interaction Tassie model, and for the two-body interactions, they used the NN realistic interaction Michigan three range Yukawa (M3Y). For some fp-shell atoms, the probability transition density B (C2) was determined. When using the Tassie model to include the CP effects, particularly at the first and second maximum momentum transfer regions, form factors were computed using the HO potential and then compared with actual results for all three maximum momentum transfer areas.

Allmond *et al.* (2014) [31]. used single step Coulomb activation of semi-magic $^{58,60,62,64}Ni$ (Z =28) beams at 1.8 MeV per nucleon on a natural carbon target to quantify with high-precision decreased electric-quadrupole transition probabilities B (E2; 0+1 2+1). The energy loss of the nickel beams through the carbon target was immediately measured with a zero-degree Bragg detector, and the exact B(E2) values were adjusted by Rutherford scattering. The B(E2) numbers don't accord with recent longevity studies that used the Doppler-shift attenuation technique.

Al-Sammarraie, *et al.*(2015)[32].studied The electron nucleus dispersion form factors for the ^{25}Mg nucleus were determined With the aid of the Woods-Saxon, harmonic oscillator, and Skyrme (Sk42) potentials, the wave functions of radial single-particle matrix elements have been computed. They discovered that the results of the inelastic transverse form factors when using the Sk42 potential agree well with the experimental data, whereas the results of the elastic magnetic scattering show a significant difference in the values when compared to the experimental

data, but the overall shape and other features of the form factors are satisfactory when using the harmonic oscillator potential.

Oleiwi and Jassim (2016)[33].studied The form factors for the inelastic electron scattering to $2^+, 4^+$ states in $^{58,60,62}Ni$ are within the context of the shell model.The computation is done in expanded $6\hbar\omega$ model space as well as $(0f_{7/2}, 1p_{3/2}, 0f_{5/2}, 1p_{1/2})$ model space.

Jassim and Faris (2017) [34]. studied The nuclear structure of ^{60}Ni was examined in terms of its energy levels, transverse form factors, charge density distribution, and transition probabilities. They used the Tassie model to compute the single particle wave function along with the Skyrme-Hartree Fock (SKX), Harmonic Oscillator (HO), and Woods-Saxon (WS) potentials.

Alzubadi (2018)[35]. studiad the nuclear structure for some odd-A nuclei ^{17}O,^{27}Al,^{39}K, and ^{51}V by using Shell model and Hartree–Fock (HF) calculations with the sd and d3f7 shell model spaces

Sarriguren *et al.* (2019)[36].studied Elastic magnetic electron scattering from distorted nuclei for ^{17}O,^{39}K, ^{25}Mg,$^{29}Si^{41}Ca$,^{51}V,^{59}Co,^{93}Nb, and ^{115}In was studied The computations are done using the Born estimate for planar waves.

Salman *et al.* (2019)[37].used the (HO) and (WS) potentials to compute the wave functions of radial single-particle matrix components in order to determine the inelastic longitudinal electron scattering form factors for $^{64,66,68}Zn$ nuclei. Results were found using the CP and NUSHELL codes with M3Y and MSDI acting as a residual interaction in order to draw theoretical inferences. They found that form factors using F5PVH interactions with WS potential are superior to those using HO Potential in all areas of momentum transmission when compared to experimental data..

Sarah J. *et al.*(2020)[38].studied investigated Using Tassie and Bohr-Mottelson, inelastic electron scattering form factors for the nuclei of

^{44}Ca,^{48}Ca,^{46}Ti, and ^{60}Ni reside in the fp-shell region. While core polarization is determined using harmonic oscillator (HO) as a leftover interaction, model computations are carried out in the fp model space using GXPF1A effective interaction.

Murshedi and Salman (2021)[39].Inelastic Longitudinal Electron Scattering Form Factors in $^{58,60}Ni$ Nuclei were investigated Murshedi and Salman using the ATBASH Code. The nucleon-nucleon realistic interaction, the Michigan three-range Yukawa interaction, and the modified surface delta interaction are used as the two-body interactions along with the F5PVH effective interaction for the fp-shell. The ^{60}Ni nuclei ultimately tend to have a greater accord than the ^{58}Ni nuclei when compared to two shell model codes for Windows, CP and OXBASH.

Jassim and Mohamed (2022)[40].studied The longitudinal Coulomb C0, C2 and C4 form factors with core-polarization effects for ^{27}Al and ^{31}p nuclei were investigated Calculations of the Core-polarization effects were done using the Coulomb Valance Tassie Model (CVTM) and the Bohr-Mottelson (BM) collective model. The wave functions of radial single particle matrix components were computed using three potentials: the Harmonic Oscillator (HO) potential, the Wood-Saxon (WS), and the SKX potential.

Majeed and sheehab (2022)[41]. studied the inelastic electron scattering form factors for several chosen states of the ^{58}Ni and $^{70,72}Ge$ nuclei that reside in the fp-shell region were examined in this research. NushellX@MSU, a recent version of the shell model code The jun45 interaction has been used to give the $1f_{5/2}2p_{1/2}1g_{9/2}$ shell model wave functions .

Obaid and Majeed(2023)[42].studied The Longitudinal and Transverse form Factors from ^{65}Cu and ^{71}Ga Nuclei, which reside in the fp-shell region, were investigated .Using jun45 effective interaction, the computation is carried out in the $(1f_{5/2}, 2p_{3/2}, 2p_{1/2}, 1g_{9/2})$ model space.In order to account for the input of the core-polarization effects, the Tassie and Bohr -Mottelson models is used, along with the proper proton and

neutron effective charges.

Alzubadi and Harby (2023)[43]. studied Calculations have been made for ^{10}B and ^{11}B for the elastic and inelastic longitudinal and transverse electron scattering form factors. To calculate the OBDM elements for low-lying positive parity states, the p-shell model space was used in the study. However, no core-shell model space with the limitation (0+1) has been employed for negative parity states according to the SPSDPF. To produce the single-particle matrix elements with the Hartree-Fock approximation and compare them to those of harmonic-oscillator and Wood-Saxon potentials, the NuShellX@MSU code was used for all computations.

Bodek and Christy(2023)[44]. studied the contribution of nuclear excitations to the Normalized Inelastic Coulomb Sum Rule $S_L(q)$ as a function of momentum transfer q and found that it is significant (0.29 ± 0.030 at q= 0.22 GeV) in Contribution of Nuclear Excitation Electromagnetic Form Factors in ^{12}C and ^{16}O to the Coulomb Sum Rule Within the uncertainty, it is discovered that the overall nuclear excitation contributions to $S_L(q)$ in ^{12}C and ^{16}O are equal.

1.3 Aim of the Present Work

In this research, the shell model calculations will be applied by using the recent version of the shell model code NushellX@MSU to calculate the electron scattering transverse form factors for some selected states of ^{51}V,^{59}Co,^{93}Nb, and ^{115}In nuclei with electron scattering longitudinal form factors for some selected states of $^{40,42,44,48}Ca$, $^{58,60,62}Ni$ nuclei lie in the fp-shell region have been investigated and comparison of theoretical calculations with available experimental data for each selected nucleus.

CHAPTER TWO

SHELL MODEL FORMALISM

2.1 Background for Shell Model

Almost every quantum mechanical problem involves Schrodinger's equation. A correct Hamiltonian is one of the most critical phases in this process. In order to write the Hamiltonian as the total of distinct components from each particle in the nucleus, it is helpful to start with the premise of independent particle motion when working with a multi-body issue like the one in nuclear physics[45].

$$H^{(0)} = \sum_{i=1}^{A} [T_i + U(r_i)] \tag{2.1}$$

Where $H^{(0)}$ is the unperturbed Hamiltonian, T_i and $U(r_i)$ are the Kinetic energy and the potential energy, respectively.Since the Pauli Exclusion Principle mandates that the wave functions for identical particles be anti-symmetric, the eigenfunctions to the above equation are given by the Slater determinant, which, for a two-particle system, is written as[45],

$$\phi_{\alpha_1\alpha_2} = \frac{1}{\sqrt{2!}} \begin{vmatrix} \varphi_{\alpha_1}(1) & \varphi_{\alpha_1}(2) \\ \varphi_{\alpha_2}(1) & \varphi_{\alpha_2}(2) \end{vmatrix} = \frac{1}{\sqrt{2!}} [\varphi_{\alpha_1}(1)\varphi_{\alpha_2}(2) - \varphi_{\alpha_1}(2)\varphi_{\alpha_2}(1)] \tag{2.2}$$

Where φ_{α_1},φ_{α_2} are the single-particle wave-functions, given the product of radial and angular components. The radial part,$R_{nl}(r)$, is the only component of this equation that is not specifically specified(r). The shape of the potential$U(r)$ of the eq.(2.1). determines the specifics of this function It turns out that selecting this possibility is not an easy decision.The mean-field potential, which is the center average potential in the shell model, is assumed to be able to approach the core. The harmonic oscillator (HO) potential with size value b, the Woods-Saxon (WS), and the Skyrme (SKX) potentials are used to generate the peripheral components of the single-nucleon wave functions used in this study. itcan be expressed as effective two-body potential[46].
Since the eigenfunctions ϕ_{ai} are well-known and integrable, choosing a HO potential is advantageous. On the other hand, a more plausible potential suggested by Woods-Saxon (WS) is not integrable, disappears at big r, and has a flat bottom.

$$U(r) = \frac{1}{2} m\omega^2 r^2 (HarmonicOscillato) \tag{2.3}$$

where m is the nucleon mass, ω is the angular frequency of the oscillator and r is the radius parameter[47].

$$U(r) = \frac{U_0}{1 + exp(\frac{r-R_0}{a})} (Woods - Saxon) \tag{2.4}$$

where U_0 is the potential depth, a is the diffuseness parameter and $R_0 = r_0 A^{\frac{1}{3}}$ The Schrödinger equation cannot replicate the shell gaps seen in nuclear data by using either of these models.A robust spin-orbit component must be added in order to correctly account for these "magic numbers." Spin-orbit interaction is a somewhat esoteric idea. It results from the inherent nucleon spin, which appears to move the nucleus around the nucleon when viewed from the viewpoint of a single nucleon traveling around the nucleus. The magnetic field created by this visible motion reacts with the nucleon's magnetic moment. The dot product of a magnetic moment and a magnetic field yields the contact energy of the two. The spin-orbit interaction energy must be proportionate to the dot product $\overrightarrow{\ell} . \overrightarrow{S}$ because the magnetic moment of the nucleon is proportional to its spin and the magnetic field resulting from the apparent motion of the nucleus is proportional to the orbital angular momentum[48].

$$U_{so} = f(r) \overrightarrow{\ell} . \overrightarrow{S} \tag{2.5}$$

Where the function $f(r)$ contains the dependence on the radial coordinate r and can be related to the central potential[23].

It is simple to see that as a system's particle count rises, so does the wave function's intricacy. Calculating the Slater determinant of equation (2.2) for three-particle, four-particle, etc. The feasibility of performing shell model computations for anything but the smallest atoms is soon put to the test by this complexity's rapid increase. Any middle or large nucleus is usually regarded in relation to the closest double-closed shell to solve this issue. The neutral nucleons are then handled separately

while the appropriately named core is assumed to be an inactive system[47].

$$\Phi_{J,\tau} \sim \Phi_{0,\tau}^{core} \times \Phi_{J,\tau}(\alpha_1, \alpha_2, ...) \tag{2.6}$$

It is now feasible to select a potential U(r) in order to fix the issue, returning to the independent-particle Hamiltonian provided by eq. (2.1) since the orbiting particles must inevitably interact with one another, the premise of independent-particle motion is incorrect in this case. Consequently, the two-particle interactions of the independent-particle Hamiltonian of an A-particle system are expressed as[47].

$$H = \sum_{k=1}^{A} T_K + \sum_{k=\ell}^{A} \sum_{\ell=k+1}^{n} W(\vec{r}_k, \vec{r}_\ell). \tag{2.7}$$

Where W $(\vec{r}_k, \vec{r}_\ell)$ is the two-body interaction between the k^{th} and th nucleons. Choosing an average potential $U_{(rk)}$, the Hamiltonian becomes,

$$H = \sum_{k=1}^{A} [T_K + U_{(rk)}] + \sum_{k=\ell}^{A} \sum_{\ell=k+1}^{n} W(\vec{r}_k, \vec{r}_\ell) - \sum_{k=1}^{A} U_{(rk)}, \tag{2.8}$$

The first component in the equation above is the same as the independent particle Hamiltonian provided by equation (2.1), and the second and third terms account for the residual interaction, or departure from independent particle motion. Equation (2.8) can be recast by dividing the summations in to core and valence contributions[47].

$$H = H_{core} + H_1 + H_2 + V(\vec{r}_1, \vec{r}_2) \tag{2.9}$$

In this case, H_{core} contains all interactions between the core nucleons, H_1 and H_2 are single-particle contributions from particles 1 and 2, and $V(\vec{r}_1, \vec{r}_2)$ is the residual interaction describing all interactions between particles 1 and 2 as well as any interactions with core nucleons. An similar formula for the energy results from using this version of the Hamiltonian in the Schrodinger equation[47].

$$E = E_{core} + E_1 + E_2 + \langle \Phi_J, \tau | V(\vec{r}_1, \vec{r}_2) | \Phi_J, \tau \rangle \tag{2.10}$$

E_{core} is the binding energy of the core nucleus, E1 and E2 are the single-particle energies of orbitals outside the core, and $\langle \Phi_J, \tau | V(\vec{r}_1, \vec{r}_2) | \Phi_J, \tau \rangle$

, is the leftover interaction in the equation above. It is crucial to understand that the energy provided by equation (2.10) only applies to pure arrangements. Any close-lying condition with the same total isospin and total rotational momentum J will combine, in theory. By combining the unperturbed wavefunctions linearly, the mixed eigenstates are obtained [47].

$$(\psi_{J,\tau})P = \sum_{k=1}^{g} a_{kp}(\Phi_{J,\tau})_k, \tag{2.11}$$

where g is the number of configurations that mix
p=1,2,...,g.

The coefficients a_{kp} provide the condition,

$$\sum_{k=1}^{g} |a_{kp}|^2 = 1 \tag{2.12}$$

Adding equation (2.11) to the Schrodinger equation results in,

$$H(\psi_{J,\tau})p = E_p(\psi_{J,\tau})p, \tag{2.13}$$

resulting in a system of linear equations[49],

$$\begin{pmatrix} H_{11} & H_{12} & \cdots & H_{1g} \\ H_{21} & H_{22} & \cdots & H_{2g} \\ \vdots & \vdots & \ddots & \vdots \\ H_{g1} & H_{g2} & \cdots & H_{gg} \end{pmatrix} \begin{pmatrix} a_{1p} \\ a_{2p} \\ \vdots \\ a_{gp} \end{pmatrix} = E_p \begin{pmatrix} a_{1p} \\ a_{2p} \\ \vdots \\ a_{gp} \end{pmatrix} \tag{2.14}$$

A common eigenvalue issue, represented by equation (2.14), is resolved by setting the determinant equal to zero[49].

$$\begin{vmatrix} H_{11} - E_p & H_{12} & \cdots & H_{1g} \\ H_{21} & H_{22} - E_p & \cdots & H_{2g} \\ \vdots & \vdots & \ddots & \vdots \\ H_{g1} & H_{g2} & \cdots & H_{gg} - E_p \end{vmatrix} = 0 \tag{2.15}$$

The end outcome is an order g polynomial in E_p with g solutions that correspond to the disturbed energies of each state that participated in the mixture. For each of the g solutions to E_p, eq.(2.14) must be solved in order to obtain the coefficients a_{kp} and subsequently the perturbed wave functions $\psi_{J,\tau}$ as each state has a distinct collection of coefficients that must be found in order to obtain the wave functions $\psi_{J,\tau}$[50].

2.1.1 Harmonic Oscillator (HO) Potential

Nuclear potential with light nuclei can be approximated by the three-dimensional oscillator potential, which is able to easily control the wave functions of individual particles. Each nucleon of mass (m) , moves separately in a potential that simulates the typical interaction with the other nucleons in a nucleus, according to the mean-field estimate. For each particle moving in a spherically symmetric harmonic oscillator potential with angular frequency (ω), assuming that the potential depth at the center of the nucleus is Uo, the Hamiltonian becomes[46]:

$$H_o = \frac{-h^2}{2m}\nabla^2 + \frac{m\omega^2 r^2}{2} - U_o \tag{2.16}$$

Where $U_o = \frac{m\omega^2 R^2}{2}$ and $R = R_0 A^{1/3}\ fm$.
The eigenvalue (Schrodinger's) equation for the wave function $\langle r, \theta, \varphi | nlm_l \rangle$ is given by[51]:

$$H_o|nlm_l\rangle = \epsilon_{nl}|nlm_l\rangle = \epsilon_{nl}|nl\rangle|lm_l\rangle \tag{2.17}$$

where the main, orbital, and magnetic quantum numbers are n, l, and m_l, respectively. The corresponding wave functions are represented by:

$$\begin{aligned} &\langle r, \theta, \varphi | nlm_l \rangle = R_{nl}(r) Y_{lm_l}(\theta, \varphi) \\ &\langle r | nl \rangle = R_{nl}(r) \\ &\langle \theta, \varphi | lm_l \rangle = Y_{lm_l}(\theta, \varphi) \end{aligned} \tag{2.18}$$

Where $Y_{lm_l}(\theta, \varphi)$ and $R_{nl}(r)$ it indicates the spherical harmonics and the radial wave functions, respectively. For the (HO) potential, the radial wave function is given by [45]:

$$\begin{aligned} R_{nl}(r) = &\sqrt{\frac{2^{l-n+3}(2l+2n-1)!!}{[(2l+1)!!]^2(n-1)!\ b^3\ \sqrt{\pi}}}\ e^{-r^2/2b^2} \\ &\sum_{k=0}^{n-1} \frac{(-1)^k\ 2^k\ (2l+1)!!}{(n-k-1)!\ k!\ (2l+2k+1)!!}(r/b)^{2k+1} \end{aligned} \tag{2.19}$$

The HO size parameter b which relates to the mass of nucleon (m) and frequency (ω) as associated with the (HO) potential[52]:

$$b = \sqrt{\frac{h/2\pi}{m\omega}} \tag{2.20}$$

The strong spin-orbit interaction component V_{ls} must be included in the single-particle Hamiltonian in order to reproduce the magic numbers [45]:

$$V_{ls} = f(r)\vec{l}.\vec{s} \tag{2.21}$$

Where $f(r)$ is a radial function, the single-particle Hamiltonian becomes:

$$H_o = \frac{-h^2}{2m}\nabla^2 + \frac{m\omega^2 r^2}{2} - U_o + f(r)\vec{l}.\vec{s} \tag{2.22}$$

The spinor state function $|Sm_s\rangle$ and the angular component of the spatial state function $|lm_l\rangle$ are coupled together in the jj coupling scheme. [53]:

$$|nljm_j\rangle = \sum_{m_l m_s} |Sm_s\rangle|nlm_l\rangle\langle lm_l Sm_s|nljm_j\rangle \tag{2.23}$$

As a result, the Single-Particle Energy (SPE) depends on the total nucleon quantum number (j), and the$\vec{l}.\vec{s}$ potential separates the (j=l+1/2) and (j=l-1/2) levels:

$$\langle nljm_j|V_{ls}|nljm_j\rangle = \langle f(r)\rangle_{nl} \begin{cases} -(l+1)/2 & for\ j = l - 1/2 \\ l/2 & for\ j = l + 1/2 \end{cases} \tag{2.24}$$

For the HO potential, the value of $\langle f(r)\rangle_{nl}$, depends on the mass number of the nucleus that is evaluated from [54]. and $\langle f(r)\rangle_{nl}$ given by:

$$\langle f(r)\rangle_{nl} = \langle nl|f(r)|nl\rangle \approx -20A^{-2/3}\ MeV \tag{2.25}$$

N$\hbar\omega$ configurations, so named because the Pauli exclusion principle permits a minimum of N oscillator quanta to be present in a shell model configuration, are possible. It is preferable to treat the proton and neutron as two charge states of a single particle known as the nucleon, disregarding their different masses. The isospin quantum number, t = 1/2, has been added in analogy with the spin quantum number,$t = \pm 1/2$, with two possible projections, t = 1/2, to differentiate the two charge states of the nucleon.As a result, the state of each nucleon defined by the quantum numbers n, l, j, m_l, t [55].

2.1.2 Woods-Saxon Potential (WS)

The (WS) potential is a fantastic choice in terms of the one-body potential. Since WS (or any other one-body potential) does not take into consideration specific two-body interactions, it cannot be used to determine the total binding energy. [52]. The (WS) parameters are used to get the optimum fit between nuclear single-particle energy and nuclear radii. The single-nucleon wave functions of the (WS) potential are given by solving the equation their radial components.[56]:

$$[-\frac{\hbar^2}{2\mu}\frac{d^2}{dr^2} + \frac{\hbar^2\, l(l+1)}{2\mu r^2} + U(r)]R(j,r) = \epsilon R(j,r) \tag{2.26}$$

Where $\mu = m(p/n)(A-1)/A$ is the reduced mass. The potential $U(r)$ include central, spin-orbital and coulomb parts and given by[57]:

$$U(r) = V_o(r) + V_{ls}(r)l.s + \delta_{pn}V^c(r) \tag{2.27}$$

Where V_o(r) is the nuclear potential depth,$V_{ls}(r)$ spin-orbit potential δ_{pn} is equal to 1 for protons and 0 for neutrons, $V^c(r)$ is the Coulomb potential. The central Woods-Saxon potential is:

$$V_o(r) = V_o[1 + exp(r - R_o)/a_o]^{-1} \tag{2.28}$$

The Coulomb potential for protons are based upon the Coulomb potential for a sphere of radius R_c given by [55]:

$$V^c(r) = \begin{cases} \frac{ze^2}{2R_c}[3 - (r/R_c)^2], & r \le R_c \\ \frac{ze^2}{r}, & r \ge R_c \end{cases} \tag{2.29}$$

The spin-orbit potential $V_{ls}(r)$ is based on the usual derivative of a Fermi shape[55]:

$$V_{ls}(r) = V_{ls}\frac{1}{r}\frac{d}{dr}[1 + exp(r + R_{ls}/a_{ls})]^{-1} \tag{2.30}$$

Where R and a are the nuclear radius, and the surface diffuseness, respectively. The radii R_o, R_{ls}, and R_c are usually expressed as:

$$R_i = r_i A^{1/3}, \quad i = 0, ls\ or\ C \tag{2.31}$$

A typical set of parameters for the WS potential are $V_o = -53Mev$, $V_{ls} = 22Mev$, $r_o = r_{ls} = 1.25fm$, $r_c = 1.20fm$ and $a_o = a_{ls} = 0.65fm$.One can find in the literature many other sets of parameters which are better for specific nuclei or mass regions[55].

2.1.3 Skyrme Interaction (SK)

In 1958, Skyrme created the Skyrme interaction[58], which can be expressed as the sum of two- and three-body parts[59]. The SK forces with the three-body term replaced by a density-dependent two-body term. The SK force can be decomposed into a central V^c, spin-orbit V_{ls} and tensor contribution V^t. V^t is usually neglected[60]. The two body term of SK force is written as a short range expansion in the form[61].

$$V^{SK} = V^c + V_{ls} + V^t \tag{2.32}$$

$$\begin{aligned} V^{SK} =& t_o(1+\chi_o\hat{p}_\sigma)\delta(\vec{r}) + \frac{1}{2}t_1(1+\chi_1\hat{p}_\sigma)(\hat{k'}^2\delta(\vec{r}) + \delta(\vec{r})\hat{k}^2) + t_2(1+\chi_2\hat{p}_\sigma) \\ & \hat{k'}\delta(\vec{r})\vec{k} + \frac{1}{6}t_3(1+\chi_3\hat{p}_\sigma)\rho^\alpha(R)\delta(\vec{r}) + it_4\hat{k'}\delta(\vec{r})(\vec{\sigma}_i + \vec{\sigma}_j) \end{aligned} \tag{2.33}$$

Where $\vec{k} = (\nabla_1 - \nabla_2)/2i$ and $\vec{k'} = (\nabla'_1 - \nabla'_2)/2i$ are relative momentum operators. $\delta(\vec{r})$ is the delta function. $\hat{p}_\sigma$ is the spin-exchange operator, σ the vector of Pauli spin matrices, and the SKyrme force parameters are $t_o, t_1, t_2, t_3, t_4, \chi_o, \chi_1, \chi_2, \chi_3$.

2.2 Tassie Collective Model(TM)

The gamma-transition and the electron excitation of nuclei have both been explained using this model. It is an inelastic scattering multiple analysis. This model is simplified to the typical liquid drop model for a uniform charge distribution. A non-uniform charge and mass density distribution is allowed by the TM model, an effort to create a model with greater flexibility and adaptation. This model states that the nucleus's ground state density affects the CP transition density. The single-particle charge density for all occupied shells, including the core, is used to construct the ground state density. The Tassie shape as shown

in eq.(2.34) [62]. provides the CP transition density in accordance with the collective modes of nuclei. For this model, the Coulomb form factor is as follows:

$$F_J^L(q) = \sqrt{\frac{4\pi}{2J_i+1}}\frac{1}{Z}\left\{\begin{array}{c} \int_0^{+\infty} r^2 j_J(qr)\rho_J^{ms}(i,f,r)dr \\ +N\int_0^{+\infty} drr^2 j_J(qr) r^{J-1}\frac{d\rho_0(i,f,r)}{dr} \end{array}\right\} F_{f.s}(q)F_{c.m}(q) \tag{2.34}$$

The radial integral $\int_0^{+\infty} drr^{J-1} j_J(qr)\frac{d\rho_0(i,f,r)}{dr}$ can be written as:

$$\int_0^{+\infty} \frac{d}{dr}\{r^{J-1} j_J(qr)\rho_0(i,f,r)\}dr$$

$$-\int_0^{+\infty} dr(J+1)r^J j_J(qr)\rho_0(i,f,r) - \int_0^{+\infty} drr^{J+1}\frac{d}{dr}j_J(qr)\rho_0(i,f,r) \tag{2.35}$$

where the first term gives zero contribution, the second and the third term can be combined together as[11]:

$$-q\int_0^{+\infty} drr^{J+1}\rho_0(i,f,r)\left[\frac{d}{d(qr)}+\frac{J+1}{qr}\right]j_{J(qr)} \tag{2.36}$$

From the recursion of spherical Bessel function[11].

$$\left[\frac{d}{d(qr)}+\frac{J+1}{qr}\right]j_{J(qr)} = j_{J-1}(qr) \tag{2.37}$$

$$\because \int_0^{+\infty} drr^{J-1} j_J(qr)\frac{d\rho_0(i,f,r)}{dr} = -q\int_0^{+\infty} drr^{J-1} j_{J-1}\rho_0(i,f,r) \tag{2.38}$$

Hence, the form factor takes the form

$$F_J^L(q) = \left(\frac{4\pi}{2J_i+1}\right)^{\frac{1}{2}}\frac{1}{Z}\left\{\begin{array}{c} \int_0^{+\infty} r^2 j_J(qr)\rho_{Jt_z}^{ms}dr \\ -Nq\int_0^{+\infty} drr^{J+1}\rho_0 j_{J-1}(qr) \end{array}\right\}\times F_{f.s}(q)\times F_{c.m}(q) \tag{2.39}$$

The proportionality constant N can be determined from the form factor at q=k

$$N = \frac{\int_0^{+\infty} drr^2 j_J(kr)\rho^{ms}_{JtZ}(i,f,r) - F^L_J Z\sqrt{\frac{2j_i+1}{4\pi}}}{k\int_0^{+\infty} drr^{J+1}\rho_0(i,f,r)j_{J-1}(kr)} \tag{2.40}$$

The form factor at the photon point q=k, is related to the transition strength B(C J) by equation (2.40), it can be shown as[11].

$$N = \frac{\int_0^{+\infty} drr^2 j_J(kr)\rho^{ms}_{JtZ}(i,f,r) - F^L_J Z\sqrt{\frac{(2j_i+1)B(CJ)}{(2J+1)!!}}k^J}{k\int_0^{+\infty} drr^{J+1}\rho_0(i,f,r)j_{J-1}(kr)}$$

$$N = \frac{\int_0^{+\infty} drr^{J+2}\rho^{ms}_{Jt_Z}(i,f,r) - \sqrt{(2J_i+1)B(CJ)}}{(2J+1)\int_0^{+\infty} drr^{2J}\rho_0(i,f,r)} \tag{2.41}$$

with $(2J+1)!! = (2J+1)(2J-1)!!$

The proportionality constant N can be determined by adjusting the reduced transition probability B(CJ) using eq. (2.41) with the experimental value of B(CJ).

2.3 Bohr-Mottelson (BM) Collective Model

It has been shown that the nucleus's ground state and several stimulated states can be accurately described by the shell model in many ways. However, it glaringly fails to account for the observed large electric quadrupole moments (Q), which are often found in the nucleus, as well as the quadrupole transition rates B(E2). The first person to attempt to explain these failings of the shall model was J. Rainwater (1950)[63]. who proposed that the mobility of the odd loose nucleon outside the core in odd A nuclei causes distortion in the shape of the

nuclear core. The even-even core becomes polarized as a result of the motion, taking on a spheroidal form. The quadrupole moment would be greater than the single-particle value as a result of this distortion. The concept was further developed by A. Bohr and B. Mottelson in (1953), who combined the single-particle and collective movements into a single model that provided a thorough explanation of the deformed nuclei [23].

Bohr and Mottelson introduced the five-dimensional (5D) quadrupole collective Hamiltonian describing the quadrupole vibrations and rotations in a unified manner. It is written as[[23],[64]]:

$$H_{coll} = T_{vib} + T_{rot} + V(\beta, \gamma) \tag{2.42}$$

$$T_{vib} = \frac{1}{2} D_{\beta,\beta}(\beta,\gamma)\dot{\beta}^2 + D_{\beta,\gamma}(\beta,\gamma)\dot{\beta}\dot{\gamma} + \frac{1}{2} D_{\gamma,\gamma}(\beta,\gamma)\dot{\gamma}^2 \tag{2.43}$$

$$T_{rot} = \frac{1}{2} \sum_{k=1}^{3} J_k(\beta,\gamma)\dot{\varphi}_k^2 \tag{2.44}$$

Where $\dot{\varphi_k}$ are the components of the rotational angle on the three intrinsic axes. The quadrupole deformation (β, γ) and the rotation angles φ_k are treated as dynamical variables, and $(\dot{\beta}, \dot{\gamma})$ represent their time-derivatives. The φ_k is called angular velocities. The quantities $(D_{\beta,\beta}, D_{\beta,\gamma}, and D_{\gamma,\gamma})$ represent inertial masses of the vibrational motion and T_{vib} represent the kinetic energies of vibrational motion.

The quantities $J_k(\beta, \gamma)$ in the rotational energy T_{rot} represent the moments of inertia with respect to the intrinsic (body-fixed) axes. This body-fixed frame, coupled with a time-dependent mean-field in real-time, can serve as a reference for defining the intrinsic axes.The term $V(\beta, \gamma)$ represent the potential energy as a function of β and γ.
The equation of the Bohr-Mottelson collective Hamiltonian from eq.(2.42) is often referred to as the liquid drop model.However, what should emphasize is that the analogy with the classical liquid drop is irrelevant to low-frequency quadrupole collective motions. Already in 1950's, it was recognized that the nucleus is "an unusual idealized quantum fluid and one is dealing with a most interesting new form of matter"[65].
Since , the vast majority of nuclei can be thought of as tiny superfluids

(with a radius of just a few femtometers), the nature of nuclear deformation is fundamentally distinct from that of surface shape oscillations in a classical liquid drop; that is, the nuclear deformation is associated with quantum shell structure and spontaneous breaking of the spherical symmetry in the self-consistent mean filed.

The form of collective Hamiltonian from eq.(2.42) is quite general and applicable to the various finite many-body systems, but values reveal the specific dynamical properties of the system of interest and the (β, γ) dependence of the collective inertia masses $(D_{\beta\beta}, D_{\beta\gamma}, D_{\gamma\gamma}, J_k)$ as well as the potential energy $V(\beta, \gamma)$.It is thus essential to extract these variables microscopically and compare them with what experimental data reveal to comprehend the dynamic features of the nucleus.
The Hamiltonian from eq.(2.42) is given in terms of the five curvilinear coordinates (β, γ and the three Euler angles which are connected with φ by a linear transformation) and their time derivatives. For quantization in curvilinear coordinates, we can adopt the so-called Pauli prescription[66].The microscopic derivation of the Bohr-Mottelson collective Hamiltonian. The quantized 5D quadrupole collective Hamiltonian takes the following form[64]:

$$\hat{H}_{coll} = \hat{T}_{vib} + \hat{T}_{rot} + V(\beta, \gamma) \tag{2.45}$$

Here, the vibrational Kinetic energy term $\hat{T}_{vib}$ is given by:

$$\begin{aligned}\hat{T}_{vib} = &-\frac{1}{2\sqrt{WR}}\{\frac{1}{\beta^4}[\frac{\partial}{\partial\beta}(\beta^2\sqrt{\frac{R}{W}}D_{\gamma\gamma}\frac{\partial}{\partial\beta}) - \frac{\partial}{\partial\beta}(\beta^2\frac{R}{W}D_{\beta\gamma}\frac{\partial}{\partial\gamma}] \\ &+ \frac{1}{\beta^2\sin(3\gamma)}(-\frac{\partial}{\partial\gamma}(\sqrt{\frac{R}{W}}\sin(3\gamma)D_{\beta\gamma}\frac{\partial}{\partial\beta})) \\ &+ \frac{\partial}{\partial\gamma}(\sqrt{\frac{R}{W}}\sin(3\gamma)D_{\beta\beta}\frac{\partial}{\partial\beta})\}\end{aligned} \tag{2.46}$$

Where the rotation energy term $\hat{T}_{rot}$ is given by:

$$\hat{T}_{rot} = \sum_{k=1}^{3}\frac{\hat{I}_k^2}{2J_K(\beta, \gamma)} \tag{2.47}$$

With $\hat{I}_k^2$ denoting three components of the angular-momentum operator with respect to the intrinsic axis. In this study, we use the unit with

$\hbar = 1$.
In the above equation[41]:

$$\beta^2 W(\beta,\gamma) = D_{\beta\beta}(\beta,\gamma)D_{\gamma\gamma}(\beta,\gamma) - D^2_{\beta\gamma}(\beta,\gamma) \tag{2.48}$$

$$R(\beta,\gamma) = D_1(\beta,\gamma)D_2(\beta,\gamma)D_3(\beta,\gamma) \tag{2.49}$$

and $D_k(\beta,\gamma)$ $(k = 1,2,3)$ are the rotational inertial functions related to the moments of inertia by[64]:

$$J_k(\beta,\gamma) = 4\beta^2 D_k(\beta,\gamma)\sin^2(\gamma - 2\pi k/3) \tag{2.50}$$

If all inertial masses $(D_{\beta\beta}, D_{\gamma\gamma}\beta^{-2}, D_1, D_2, D_3)$ are replaced by a common constant:
D and $D_{\beta\gamma}$ is ignored, the above $\hat{T}_{vib}$ is reduced to:

$$\hat{T}_{vib} = -\frac{1}{2D}\left(\frac{1}{\beta^4}\frac{\partial}{\partial\beta}\beta^4\frac{\partial}{\partial\beta} + \frac{1}{\beta^2\sin(3\gamma)}\frac{\partial}{\partial\gamma}\sin(3\gamma)\frac{\partial}{\partial\gamma}\right) \tag{2.51}$$

Only small-amplitude vibrations around a spherical Hartree-Fock Bogoliubov (HFB) equilibrium may be valid for such a drastic approximation in this context. The need to go beyond this simplest approximation for the inertia masses has been pointed out[23].For recent experimental data and phenomenological analyses of this problem[66].
The collective Schrodinger equation is[41][23]:

$$\left(\hat{T}_{vib} + \hat{T}_{rot} + V(\beta,\gamma)\right)\psi_{\alpha IM}(\beta,\gamma,\Omega) = E_{\alpha I}\,\psi_{\alpha IM}(\beta,\gamma,\Omega) \tag{2.52}$$

The collective wave function in the laboratory frame, $\psi_{\alpha IM}(\beta,\gamma,\Omega)$ is the function of β,γ and Ω set of three Euler angles Ω. It is specified by the total angular momentum I, its projection onto the z-axis in the laboratory frame M, and α the distinguishes the eigenstates possessing the same value of I and M. With the rotational wave function D^I_{MK}, they are written as[64]:

$$\psi_{\alpha IM}(\beta,\gamma,\Omega) = \sum_{k=even}\phi_{\alpha Ik}(\beta,\gamma)\langle\Omega|IMK\rangle \tag{2.53}$$

Where

$$\langle\Omega|IMK\rangle = \sqrt{\frac{2I+1}{161\pi^2(1+\delta_{k_0}}}[D^I_{MK}(\Omega) + (-1)^I D^I_{M,-k}(\Omega)] \tag{2.54}$$

The vibration wave functions in the body-fixed frame,$\phi_{\alpha IK}(\beta,\gamma)$, are normalized as:

$$\int d\beta\, d\gamma\, \sqrt{G(\beta,\gamma)}\, |\phi_{\alpha I}(\beta,\gamma)|^2 = 1 \tag{2.55}$$

Where

$$|\phi_{\alpha I}(\beta,\gamma)|^2 = \sum_{k=even} |\phi_{\alpha Ik}(\beta,\gamma)|^2 \tag{2.56}$$

and the volume element is given by $\sqrt{G(\beta,\gamma)}\, d\beta\, d\gamma$ with:

$$G(\beta,\gamma) = 4\beta^8 W(\beta,\gamma) R(\beta,\gamma) \sin^2(3\gamma) \tag{2.57}$$

Thorough discussions of symmetries of the collective wave functions and the boundary condition for solving the collective Schrodinger equation are given in Refs[67][68].
Inserting (2.53) into the collective Schrodinger equation (2.52), we obtain the egenvalue equation for vibrational wave functions[69].

$$\begin{aligned}[\hat{T}_{vib} + V(\beta,\gamma)]\phi_{\alpha IK}(\beta,\gamma) + \sum_{k'=even} \langle IMK|\hat{T}_{rot}|IMK'\rangle \phi_{\alpha IK'}(\beta,\gamma) \\ = E_{\alpha I}\ \phi_{\alpha IK}(\beta,\gamma)\end{aligned} \tag{2.58}$$

Solving this equation, we obtain quantum spectra and collective wave functions.

CHAPTER THREE

GENERAL THEORY

3.1 General Theory

According to the Plane-Wave Born Approximation (PWBA), the cross section for unpolarized electron scattering from initial nuclear state i to final nuclear state f is given by[11][70][71]:

$$\frac{d\sigma}{d\Omega} = \sigma_M \, \eta^{-1} \left\{ \left(\frac{q_\mu}{q}\right)^4 F_L^2(q) + \left[\frac{1}{2}\left(\frac{q_\mu}{q}\right)^2 + tan^2\left(\frac{\theta}{2}\right)\right] F_T^2(q) \right\}, \quad (3.1)$$

Where σ_M is the Mott cross-section for scattering from a point like nuclear charge Ze and is defined as[12]:

$$\sigma_M = \left[\frac{Z\alpha \cos(\theta/2)}{2E_i sin^2(\theta/2)}\right]^2, \quad (3.2)$$

Where Z is the atomic number of the target nucleus,E_i is the energy of the input electron, and θ is the angle of scattering. $\alpha = e^2/hc = 1/137$ is the fine structure constant. The nucleus's recoil factor is determined by [11]:

$$f_{rec} = [1 + \frac{2E_i}{M} sin^2(\theta/2)]^{-1} \quad (3.3)$$

Where E_i is the incident electron energy, E' is the scattering electron energy, q is the three-momentum transfer, and q_μ is the four-momentum transfer, which together make up the energy transfer $\omega = E_i - E'$, [11]:

$$q_\mu^2 = q^2 - \omega^2 = 4EE' sin^2(\theta/2) \quad (3.4)$$

The form factor is given by the well-known multi-pole as a function of momentum transfer q, [72]:

$$|F_J^\eta(q)|^2 = \frac{4\pi}{Z^2(2J_i+1)} |\langle J_f \| \hat{T}_J^\eta(q) \| J_i \rangle|^2 \quad (3.5)$$

In the electron scattering multi-pole operator $T_J^\eta(q)$, the superscripts T and L stand for transverse (T) and longitudinal (L), respectively. J_i and J_f stand for the total angular momentum of the initial and final states. The form factor can be expressed in terms of a matrix element

that is reduced to contain both the angular momentum (J) and isospin (T) when the Wigner-Eckert theory is applied in the isospin space. :

$$|F_J^{\eta}(q)|^2 = \frac{4\pi}{Z^2(2J_i+1)} \Big| \sum_{T=0,1} (-1)^{T_f - T_{zf}} \begin{pmatrix} T_f & T & T_i \\ -T_{Zf} & M_T & T_{Zi} \end{pmatrix} \langle J_f T_f \| \hat{T}^{\eta}_{JT}(q) \| J_i T_i \rangle \Big|^2 \tag{3.6}$$

Where $T_Z = |\frac{Z-N}{2}|$

The rule of angular momentum and isospin can be written as:

$$|J_i - J_f| \leq J \leq J_i + J_f \tag{3.7}$$

$$|T_i - T_f| \leq T \leq T_i + T_f \tag{3.8}$$

And the parity selection rules:

$\pi_i \pi_f = (-1)^J$ for CJ and EJ multi-poles

$\pi_i \pi_f = (-1)^{J+1}$ for MJ multi-poles

where CJ, EJ, and MJ stand for Coulomb, electric, and magnetic multi-poles, respectively.

3.2 The Reduced Single-Particle Matrix Elements

The reduced matrix element of the necessary operator T^{η}_{Λ} is defined as the product of the elements of the One Body Density Matrix (OBDM) times the elements of the single particle-matrix. [73]:

$$\langle J_f \| \hat{T}^{\eta}_{J,t_Z} \| J_i \rangle = \sum_{a,b} OBDM^{J,t_Z}(J_i, J_f, a, b) \langle a \| \hat{T}^{\eta}_{J,t_Z} \| b \rangle \tag{3.9}$$

where $t_z = \frac{1}{2}$ for proton and $-\frac{1}{2}$ for neutron. The initial and final states of the nucleus are statesJi and Jf, respectively, where J denotes multi-polarity. The decreased matrix element in spin space is shown by the double bar $\langle \| \rangle$. determines whether to use the longitudinal or Coulomb (Col.), transverse electric(el..), or magnetic(mag) operators, accordingly.The end and starting states are represented by the single-particle states a and b, respectively. [73]:

$$|a\rangle = |n_a l_a\rangle |j_a m_a\rangle |t t_z\rangle \tag{3.10}$$

$$|b\rangle = |n_b l_b\rangle |j_b m_b\rangle |tt_z\rangle \tag{3.11}$$

The total single-particle angular momentum quantum numbers are (j_a,j_b), the principle quantum numbers are (n_a,n_b), the orbital angular momentum numbers are l_a, l_b), the projection of (j_a,j_b) is (m_a,m_b) , and the single-particle isospin state is $|tt_z\rangle$.

3.3 The One Body Density Matrix Elements (OBDM)

The work of Lee and Kurath is where the OBDM components come from [74]: The transition amplitudes are connected to the OBDM components employed in this study By $A_{J,t_z}(j_a, j_b)$,

$$OBDM^{J,t_z}(i, f, j_a, j_b) = \sqrt{2J_f + 1}\frac{A_{J,t_z}(j_a, j_b)}{\sqrt{2J+1}} \tag{3.12}$$

The transformation from L-S coupling basis to J-J coupling is given by[74]:

$$A_{J,t_z}(j_a, j_b) = \sum_{LS}(\hat{j_a}\hat{j_b}\hat{L}\hat{S})^{1/2} \begin{Bmatrix} l_b & 1/2 & j_b \\ l_a & 1/2 & j_a \\ L & S & J \end{Bmatrix} A_{J,t_z}(LS) \tag{3.13}$$

Where the bracket $\begin{Bmatrix} .... \\ .... \\ .... \end{Bmatrix}$ is the 9j-symbols and $\hat{J} = 2J+1$. In isospin representation, the value of the $OBDM^{J,T}$ is obtained from the value of $OBDM^{J,t_z}$ as[62]:

$$\begin{aligned} OBDM^{J,t_z} =& (-1)^{T_f - T_z}\Bigg\{\sqrt{2}\begin{pmatrix} T_f & 0 & T_i \\ -T_Z & 0 & T_Z \end{pmatrix}\frac{OBDM(\Delta T = 0)}{2} + 2t_z\sqrt{6} \\ & \begin{pmatrix} T_f & 0 & T_i \\ -T_Z & 0 & T_Z \end{pmatrix}\frac{OBDM(\Delta T = 1)}{2}\Bigg\} \end{aligned} \tag{3.14}$$

With $t_z = \frac{1}{2}$ for a proton and $\frac{-1}{2}$ for a neutron. The bracket $\begin{pmatrix} .... \\ .... \end{pmatrix}$ is 3j-symbol.

3.4 The Longitudinal Operator's Reduced Single-Particle Matrix Elements

The only nucleon that is thought to interact with the electron in the single-particle model is one that is in a state with a well defined shell model. The longitudinal scattering results from the interaction of electrons with the charge distribution of the nucleus, as described by the longitudinal (Coulomb) form factors. In the nuclear Hilbert space, the longitudinal operator, an irreducible operator of rank J, is defined as[11]:

$$\hat{T}^{L}_{J,M}(q,t_z) = \int d\vec{r}\; j_J(qr)\; Y_{JM}(\Omega_r)\; \hat{\rho}(\vec{r},t_z) \tag{3.15}$$

Where $j_J(qr)$ is the spherical Bessal function, $Y_{JM}(r)$ is the spherical harmonic and $\hat{\rho}(\vec{r},t_z)$ is the single nucleon charge density operator is given by[49]:

$$\hat{\rho}(\vec{r},t_z) = e(t_z)\delta(\vec{r}-\vec{r_i}) \tag{3.16}$$

Where $\delta(\vec{r}-\vec{r_i})$ is Dirac deita function and $e(t_z) = \frac{1+2t_z}{2}$. From the equations (3.15) and (3.16), then equation (3.15) becomes:

$$\hat{T}_{J,M}(q,t_z) = e(t_z)\; j_J(qr)\; Y_{JM}(\Omega_r) \tag{3.17}$$

Between the initial $|n_b,l_b,j_b\rangle$ and final $|n_a,l_a,j_a\rangle$ states, the reduced single-particle matrix element's longitudinal operator may be written as[11]:

$$\begin{aligned}\langle n_a,l_a,j_a\|\hat{T}_{J,t_z}\|n_a,l_a,j_a\rangle =& e(t_z)\langle n_a,l_a|j_J(qr)|n_a,l_a\rangle \\ & \left\langle l_a\frac{1}{2}\; j_a\|Y_J(\Omega_r)\|l_b\frac{1}{2}\; j_b\right\rangle\end{aligned} \tag{3.18}$$

The reduced matrix elements of the spherical harmonic are [71]:

$$\begin{aligned}\langle l_a\frac{1}{2}\; j_a\|Y_J(\Omega_r)\|l_b\frac{1}{2}\; j_b\rangle =& \frac{1}{2}(-1)^{j_a+1/2}[1+(-1)^{l_a+l_b+J}] \\ & \sqrt{\frac{(2j_a+1)(2j_b+1)(2J+1)}{4\pi}}\begin{bmatrix} j_a & J & j_b \\ 1/2 & 0 & -1/2\end{bmatrix}\end{aligned} \tag{3.19}$$

The single-particle matrix element of the spherical Bessel's function is[75]:

$$\langle n_a l_a | j_J(qr) | n_b l_b \rangle = \int_0^\infty dr r^2 j_J(qr) R_{n_a,l_a}(r) R_{n_b,l_b}(r) \tag{3.20}$$

the radial component of the single-particle wave function are $R_{n_a,l_a}(r)$ and $R_{n_b,l_b}(r)$. The size parameter b of the Harmonic Oscillator (HO) potential, which is used, allows for the analysis of the radial matrix elements of the Bessel function as [73]:

$$\begin{aligned}\langle n_a l_a | j_J(qr) | n_b l_b \rangle =& \frac{2^J}{(2J+1)!!} Y^{J/2} exp(-Y)[(n_b-1)!(n_a-1)!]^{1/2} \\ & [\Gamma(n_b+l_b+1/2)\Gamma(n_a+l_a+1/2)]^{1/2} \sum_{m_b=0}^{n_b-1} \sum_{m_a=0}^{n_a-1} \\ & \frac{(-1)^{(m_b+m_a)}}{m_a! m_b!} \frac{1}{(n_{b-m_b}-1)!(n_a-m_a-1)!} \\ & \frac{\Gamma(1/2(l_b+la+2m_b+2m_a+J+3)}{\Gamma(m_b+l_b+3/2)\Gamma(m_a+l_a+3/2)} \\ & F(1/2(J-l_a-l_a-2m_b-2m_a); J+3/2; Y)\end{aligned} \tag{3.21}$$

Where $Y = (bq/2)^2$., Γ is gamma function and F is the confluent hypergeometric function, which may be evaluated by using[73]:

$$F(\alpha;\beta;\gamma) = 1 + \frac{\alpha}{\beta}\gamma + \frac{\alpha(\alpha+1)}{\beta(\beta+1)}\frac{\gamma^2}{2!} + ... \tag{3.22}$$

It is possible to express the longitudinal form factor in terms of the reduced many-particles matrix element of the transition operator as[45]:

$$|F^L_{J,t_z}(q)|^2 = \frac{1}{z^2}\frac{4\pi}{2J_i+1}\langle J_f \| \hat{T}^L_{Jt_z} \| J_i \rangle \tag{3.23}$$

The reduced many-partical matrix element with spin-space is given by[73]:

$$\langle J_f \| \hat{T}^L_{Jt_z} \| J_i \rangle = \sum_{a,b} OBDM(J_f, J_i, a, b, J, t_z) \langle a \| \hat{T}^L_{Jt_z} \| b \rangle \tag{3.24}$$

Also, it may be expressed as[73]:

$$\langle J_f \| \hat{T}^L_{Jt_z} \| J_i \rangle = e(t_z) \int_0^\infty dr r^2 j_J(qr) \rho_{Jt_z}(i,f,r) \tag{3.25}$$

Where ρ_{Jt_z} is the transition charge density and given by.[73]:

$$\rho_{Jt_z}(r) = \sum_{a,b} OBDM^{Jt_z}(i,f,a,b) \langle n_a l_a j_a \| Y_J \| n_b l_b j_b \rangle R_{n_a l_a}(r) R_{n_b l_b}(r), \tag{3.26}$$

Two adjustments are made to the nuclear form factors, both of which are reflected in eq. (3.25). The finite nucleon size (f.s) correction and the center-of-mass (c.m) correction are calculated as [76]:

$$F_{f.s}(q) = e^{\frac{-0.43q^2}{4}} \tag{3.27}$$

$$F_{c.m}(q) = e^{\frac{q^2 b^2}{4A}} \tag{3.28}$$

Where b is the Harmonic-Oscillator size parameter and A is the nuclear mass number. The center of mass is corrected to remove the false states that appear when applying a shell model wave function. Calculating the form factor requires taking into account the effects of a restricted nucleus size, center of mass motion, and Coulomb distortion of electron waves.Consequently, utilizing Wigner-Eckart theory and the multi-polarity J's form factor as reduced matrix components in the angular momentum and isospin spaces[24]:

$$\begin{aligned} |F^\eta_J(q)|^2 =& \frac{4\pi}{Z^2(2J_i+1)} | \sum_{T=0,1} (-1)^{T_f - T_z f} \begin{pmatrix} T_f & T & T_i \\ -T_{Zf} & M_T & T_{Zi} \end{pmatrix} \\ & \langle \Gamma_f \| | \hat{T}^\eta_{J,T}(q) \| | \Gamma_i \rangle | F_{f.s}(q)|^2 |F_{c.m}(q)|^2 \end{aligned} \tag{3.29}$$

Where $T_z = \frac{Z-N}{2}$.
The single-particle energies are given by[45]:

$$e_{nlj} = (2n + l - 1/2)\hbar\omega + \begin{cases} -1/2(l+1)\langle f(r) \rangle_{nl} & for\ j = l - 1/2 \\ 1/2l \langle f(r) \rangle_{nl} & for\ j = l + 1/2 \end{cases} \tag{3.30}$$

With

$$\begin{aligned} \langle f(r) \rangle_{nl} \approx & 20 A^{-2/3} Mev, \\ & \hbar\omega = 45 A^{-1/3} - 25 A^{-2/3} \end{aligned} \tag{3.31}$$

Electron Coulomb distortions increase the momentum transfer to first order, producing an efficient transfer q_{eff} f that is given by[70] [77]:

$$q_{eff} = q[1 + \frac{3}{2}\frac{Ze^2}{ER_c}] \tag{3.32}$$

Where $R_c = \sqrt{\frac{5}{3}}R_{rms}$ is the root mean square (rms) charge radius.

3.5 The Electromagnetic Transition Probability

At the photon point, when the momentum transfer $q = k = E_x/\hbar c$, occurs, the electromagnetic transition probability is determined.where E_x is the excitation energy.The form factor at (q=k) is [24]:

$$|F_J^L(k)|^2 = \frac{4\pi}{(2J_i+1)Z^2}\left|\int_0^\infty dr\, r^2 j_J(kr)\rho_J(i,f,r)\right|^2, \tag{3.33}$$

Hence, for this value of q, the center of mass and finite nucleon size correction factors are roughly equal to one. At $q = k = E_x/\hbar c$

$$j_J(kr) = \frac{(kr)^J}{(2J+1)!!}(1 - \frac{1}{2}\frac{(kr)^J}{(2J+3)} + ...) \tag{3.34}$$

Retaining only the leading term in the series expansion of $j_J(kr)$, one obtains:

$$j_J(kr) \approx \frac{(kr)^J}{(2J+1)!!} \tag{3.35}$$

Then equation (3.33) becomes:

$$|F_J^L(k)|^2 = \frac{4\pi}{(2J_i+1)Z^2}\left[\frac{(k)^J}{(2J+1)!!}\right]^2\left|\int_0^\infty dr\, r^{J+2}\rho_J(i,f,r)\right|^2 \tag{3.36}$$

The definition of the multi-pole matrix element is[78]

$$Q_{f_i}^J = \int_0^\infty dr\ r^{J+2}\rho_J(i,f,r) \tag{3.37}$$

Hence the reduced transition probability is described as follows:

$$B(CJ) = \frac{|Q_{f_i}^J|^2}{2J_i + 1} \tag{3.38}$$

Afterward, the diminished transition probability B(CJ) is expressed as follows using the form factor at the photon point[24]:

$$B(CJ) = \frac{[(2J+1)!!]^2 Z^2 e^2}{4\pi k^{2J}} |F_J^L(k)|^2 \tag{3.39}$$

In the PWBA, the longitudinal form factor is given by Fourier transformation of the transition density $\rho_{fi}(r)$[11]:

$$|F_c(q)|^2 = \frac{1}{Z^2} \sum_{M_i, M_f} |\rho(q)|^2, \tag{3.40}$$

Where

$$\rho(q) = \int e^{iq.r} \langle J_f M_f | \hat{\rho}(r) | J_i M_i \rangle dq \tag{3.41}$$

The Dirac delta function and the one-body density operator $\hat{\rho}^{(1)}(\vec{r})$ may be used to represent the density distribution of an A-point nucleon system as [79]:

$$\hat{\rho}^{(1)}(\vec{r}) = \sum_{i=1}^{A} \delta(\vec{r} - \vec{r_i}) e_i. \tag{3.42}$$

The many-particle wave function ψ may be used to define the expected value for the one-body density operator and is written as [72]:

$$\begin{aligned} \langle \psi(\vec{r}_1, \vec{r}_2, ...\vec{r}_A) | \hat{\rho}^{(1)}(\vec{r}) | \psi(\vec{r}_1, \vec{r}_2, ...\vec{r}_A) \rangle = & \sum_{i=1}^{A} \int_0^{\infty} \psi^*(\vec{r}_1, \vec{r}_2, ...\vec{r}_A) \delta(\vec{r} - \vec{r_i}) \\ & \psi(\vec{r}_1, \vec{r}_2, ...\vec{r}_A) d\vec{r}_1 d\vec{r}_2 ... d\vec{r}_A \end{aligned} \tag{3.43}$$

In terms of Slater determinants and as shown by, the single-particle wave function $\phi_i(\vec{r_j})$ may be used to represent the nuclear many-particle wave function ψ . [72]:

$$\psi(\vec{r}_1, \vec{r}_2, ...\vec{r}_A) = \frac{1}{\sqrt{A!}} det \phi_i(\vec{r_j}) \tag{3.44}$$

The integration over the coordinates then results in [72]

$$\rho_o(r) = \langle \psi(\vec{r}_1, \vec{r}_2, ...\vec{r}_A) | \hat{\rho}^{(1)}(\vec{r}) | \psi(\vec{r}_1, \vec{r}_2, ...\vec{r}_A) \rangle \tag{3.45}$$

As a result, the single-particle wave function may be used to calculate the density distribution of a system containing A nucleons as[80]:

$$\rho_o(r) = \sum_{i=1}^{A} |\phi_i(\vec{r})|^2 \tag{3.46}$$

We will operate with a Harmonic Oscillator basis and define our single particle states as follows in order to derive an explicit formula for the one body density matrix elements: :

$$\phi_i(\vec{r}) = \psi_{nlm}(\vec{r}) \chi_{si} \chi_{ti}, \tag{3.47}$$

Where $i = n, l, m, s_i, t_i$ while $\psi_{nlm}(\vec{r})$, χ_{si}, and χ_{ti} are space, spin, and isospin wave functions, respectively. The space wave function of (HO) is given by:

$$\psi_{nlm}(\vec{r}) = R_{nl}(r) Y_{lm}(\theta_i, \phi_i) \tag{3.48}$$

The equation (3.46) can be written as,[72]:

$$\rho_o(r) = \sum_{nlm} |\psi(\vec{r})|^2 . \sum_{s_i, t_i} |\chi_{si} \chi_{ti}|^2 \tag{3.49}$$

$$\rho_o(r) = \sum_{nlm} |R_{nl}(r) Y_{lm}(\theta_i, \phi_i)|^2 . \sum_{s_i, t_i} |\chi_{si} \chi_{ti}|^2 \tag{3.50}$$

$$\rho_o(r) = 4 \sum_{nl} |R_{nl}(r)|^2 . \sum_{m} |Y_{lm}(\theta_i, \phi_i)|^2 \tag{3.51}$$

where the factor 4 in equation (3.51) takes into account the spin-isospin degeneracy i.e.., The charge density distribution does not depend on the s_i and t_i, therefore these indices have been neglected by summing over the projections m_s and m_t to obtain the factor 4. The second factor of equation (3.51) can be written as,[72]:

$$\sum_{m} |Y_{lm}(\theta_i, \phi_i)|^2 = \frac{2l+1}{4\pi} \tag{3.52}$$

The density of the system (A) nucleons written as[72]:

$$\rho_o(r) = 4\sum_{nl} |R_{nl}(r)|^2 .\frac{2l+1}{4\pi} \tag{3.53}$$

As a result, for closed shell nuclei with Z=N, the ground charge density distribution is given by[72]:

$$\rho_o(r) = 2\sum_{nl} \left(\frac{2l+1}{4\pi}\right)|R_{nl}(r)|^2 \tag{3.54}$$

The charge density at ground state may be written as for open shell nuclei.:

$$\rho_o(r) = \frac{1}{4\pi}\sum_{nl\in I} 2(2l+1)|R_{nl}(r)|^2 + \frac{1}{4\pi}\sum_{nl\notin I} N_p|R_{nl}(r)|^2 \tag{3.55}$$

Where I: closed shell N_p , number of protons in the unfilled orbit's and $R_{nl}(r)$ is given by:

$$\begin{aligned} R_{nl}(r) =& \frac{1}{(2l+1)!!}[\frac{2^{l-n+3}(2n+2l-1)!!}{b^3\sqrt{\pi}(n-1)!}]^{1/2}\,(r/b)^l\, e^{-r^2/b^2} \\ & {}_1F_1(1-n, l+\frac{3}{2}; \frac{r^2}{b^2}) \end{aligned} \tag{3.56}$$

${}_1F_1(1-n, l+\frac{3}{2}; \frac{r^2}{b^2})$ is the confluent hyper-geometric series and is given by[72]:

$${}_1F_1(1-n, l+\frac{3}{2}; \frac{r^2}{b^2}) = \sum_{k=1}^{n-1}(-1)^k \frac{(n-1)!2^k}{(n-k-1)!k!}\frac{(2l+1)!!}{(2l+2k+1)!!}(r/b)^{2k} \tag{3.57}$$

With n!!=n(n-1)(n-4)....(2 or 1),
n!=n(n-1)(n-2)....1
b is the harmonic oscillator size parameter is given by[72]:

$$b = 1.005A^{1/6}\ \ fm \tag{3.58}$$

Size parameter b is dependent on the nuclear mass number A, which is the case for HO wells...

CHAPTER FOUR

RESULTS ,DISCUSSION AND CONCLUSIONS

4.1 Introduction

Calculations need the use of mathematics, quantum mechanical theories, and nuclear shell model theories and formulas. To carry out such extensive calculations. These many issues must be programmed into a computer program to perform such a massive computations[81].The nuclear shell model has shown to be a highly useful tool for studying the nuclear structure because it can precisely and systematically account for a variety of observables by selecting an appropriate residual effective interaction. The nuclear shell model was created as the understanding of nuclear structure advanced. The shell model, although being essentially straightforward, explains a number of nuclear phenomena, including spin, magnetic moment, and nuclear spectra. The shell model is made up of two key types of models that are connected to its foundation: the models of the mean field and they configuration mixing models[9].

To compare the theoretical results with experimental data In this work, large-scale(and restriction) shell-model calculations were performed. The shell model code NuShellX@MSU [16] was used, with the d3f7, ho, jj44, glekpn model space was utilised,including $d_{3/2}$, $f_{7/2}$, $p_{3/2}$, $f_{5/2}$, $p_{1/2}$,$g_{9/2}$ for protons and neutrons.The core polarization effects (CP) are calculated with (ho, w0, jj44b and glekpn) as effective residual interactions. The HO, WS and SKX potential have been used to calculate the wave functions of the single-particle matrix elements, ten nuclei ($^{58,60,62}Ni$, $^{42,44,48}Ca$, ^{51}V,^{59}Co, ^{93}Nb and ^{115}In) were considered in this work .The calculations presented here were performed using Bohr-Mottelson ,valence and Tassie models .

4.2 The Transverse Form Factors Calculations

4.2.1 The nucleus ^{51}V

The vanadium (^{51}V) nucleus contains 23 protons and 28 neutrons.Thus, it contains 3 protons outside the core ^{48}Ca distributed over the f-shell space, To describe the experimental data [82, 83, 84], we need to consider the total contribution of M1, M3, M5, and M7 multi-poles. The shell model calculations are performed using d3f7 model space whit (w0) effective interaction. Figure (4.1) shows The total magnetic form factor that the total contribution of M1(whit WS3 potential) , M3(whit WS3 potential),M5(whit WS3 potential),and M7(whit SK35 potential) for $^{51}V(J^{\pi} = \frac{7}{2}^{-})$ is shown in red, blue, green, and yellow, respectively by using the valence with (b)and without(a) core polarization effects models . In the first peak between $(0 \leq q \leq 1.5)fm^{-1}$, the dominant component is M1 where the maximum values are 10^{-3} and $0.6fm^{-1}$ for form factors and momentum transfer values respectively.At the second peak between $(1.5 \leq q \leq 3)fm^{-1}$, the dominant component is M7 where the maximum values are 10^{-4} and $3fm^{-1}$ for form factors and momentum transfer values respectively ,there is no rapprochement between the experiment's and the theoretical data for the final peak.

Figure (4.1) section (c) shows the total magnetic form factor for The nucleus ^{51}V , as it appears with polarization in red and without polarization in blue, respectively. From the figure, we conclude that the polarization is minimal or almost non-existent.

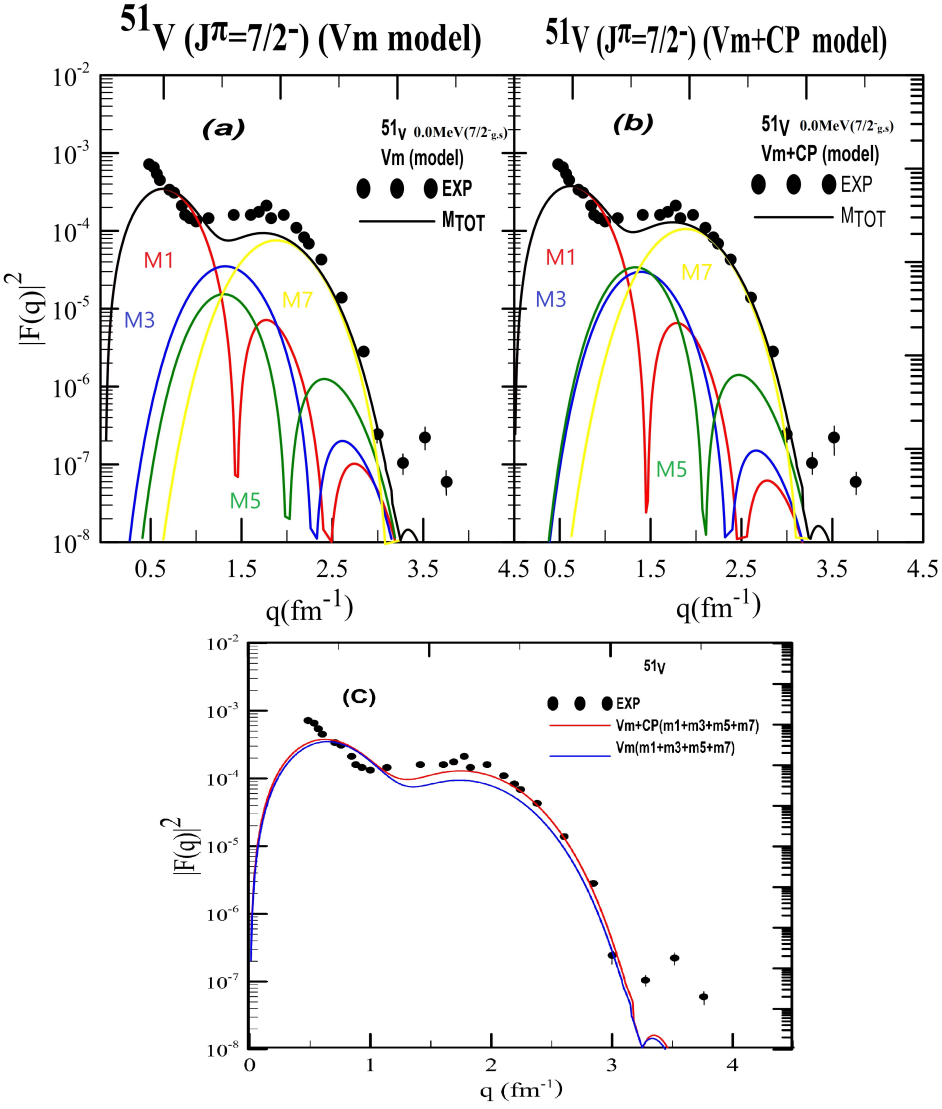

Figure 4.1: The total transverse magnetic form factor for the transition to the $(\frac{7}{2}^{-})$ state in the ^{51}V nucleus, without(a),with (b) core-polarization effects and (c)the relation between momentum transfer q and total magnetic form factor, as it appears with polarization in red and without polarization in blue, respectively. The experimental data are taken from ref.[82, 83, 84].

4.2.2 The nucleus ^{59}Co

The ^{59}Co nucleus has 27 protons and 32 neutrons. The ^{59}Co nucleus has 11 nucleons outside the core.^{48}Ca The experiment data for ^{59}Co nucleus taken from the ref[82, 85, 86].To describe the experimental data, we need to consider the total contribution of M1, M3, M5, and M7 multipoles. The shell model calculations are performed using (ho) model space wiht (ho) effective interaction. Figure (4.2) shows The total magnetic form factor that the total contribution of M1(wiht WS3 potential) , M3(wiht sk33 potential) , M5(wiht Ho potential) , and M7(wiht Ho potential) . It was applied to the fp-shell model space wave function. for $^{59}Co(J^{\pi} = \frac{7}{2})$ is shown in red, blue, green, and yellow, respectively by using the Valence With (b)and Without(a) core polarization effects models .In the first peak between $(0 \leq q \leq 1.3)fm^{-1}$, the dominant component is M1 where the maximum values are 10^{-3} and $(0.7)fm^{-1}$ for form factors and momentum transfer values respectively ,At the second peak between $(1.5 \leq q \leq 3.4)fm^{-1}$, the dominant component is M7 where the maximum values is 10^{-4} and $(2.3)fm^{-1}$ for form factors and momentum transfer values respectively.

Figure (4.2) section (c) shows the total magnetic form factor for The nucleus ^{59}Co , as it appears with polarization in red and without polarization in blue, respectively. From the figure, we conclude that the polarization is minimal or almost non-existent.

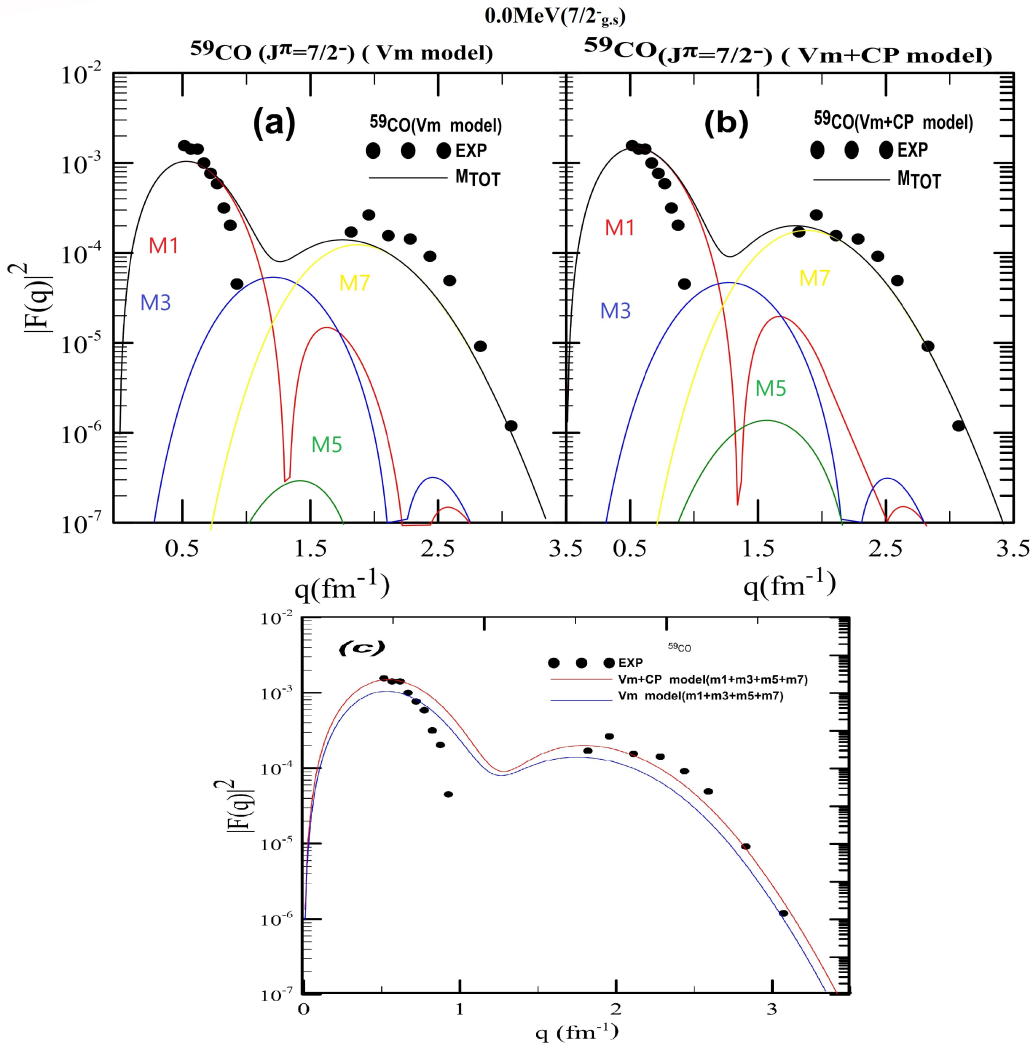

Figure 4.2: The total transverse magnetic form factor for the transition to the $(\frac{7}{2}^{-})$ state in the ^{59}Co nucleus, without(a),with (b) core-polarization effects and,(c) the relation between momentum transfer q and total magnetic form factor, as it appears with polarization in blue and without polarization in red, respectively. The experimental data are taken from ref. [82, 85, 86].

4.2.3 The nucleus ^{93}Nb

The transverse form factor calculations have been performed in the (glekpn with restriction) model space with the shell-model code NUSHELL X@MUS since we are interested in the positive-parity states of ^{93}Nb for the valance particles states (1g 9/2) outside the core ^{56}Ni, The Vm(a) and the Vm with CP model(b) are compared as the total magnetic form factor, which symbolizes the sum. The contribution of M1, M3, M5, and M7 for ^{93}Nb ($J^{\pi} = \frac{9}{2}^{+}$) is shown in red, blue, green, and yellow, respectively. Effective interaction *glekpn*. It was applied to the g-shell model space wave function. In the first peak between $(0 \leq q \leq 1.1)fm^{-1}$, the dominant component is M1 where the maximum values are 10^{-3} and $(0.6)fm^{-1}$ for form factors and momentum transfer values respectively ,At the second peak between $(1.4 \leq q \leq 3)fm^{-1}$, the dominant component is M3 where the maximum values are 10^{-3} and $(1.7)fm^{-1}$ for form factors and momentum transfer values respectively.

Figure (4.3) section (c) compares the total magnetic form factor between the Valence model(Vm),shown in blue line ,and the Valence model with core polarization(Vm+Cp), shown in red line.It is clear from the peaks in the figure that the core effect is very small, because the form factor in our work is transverse

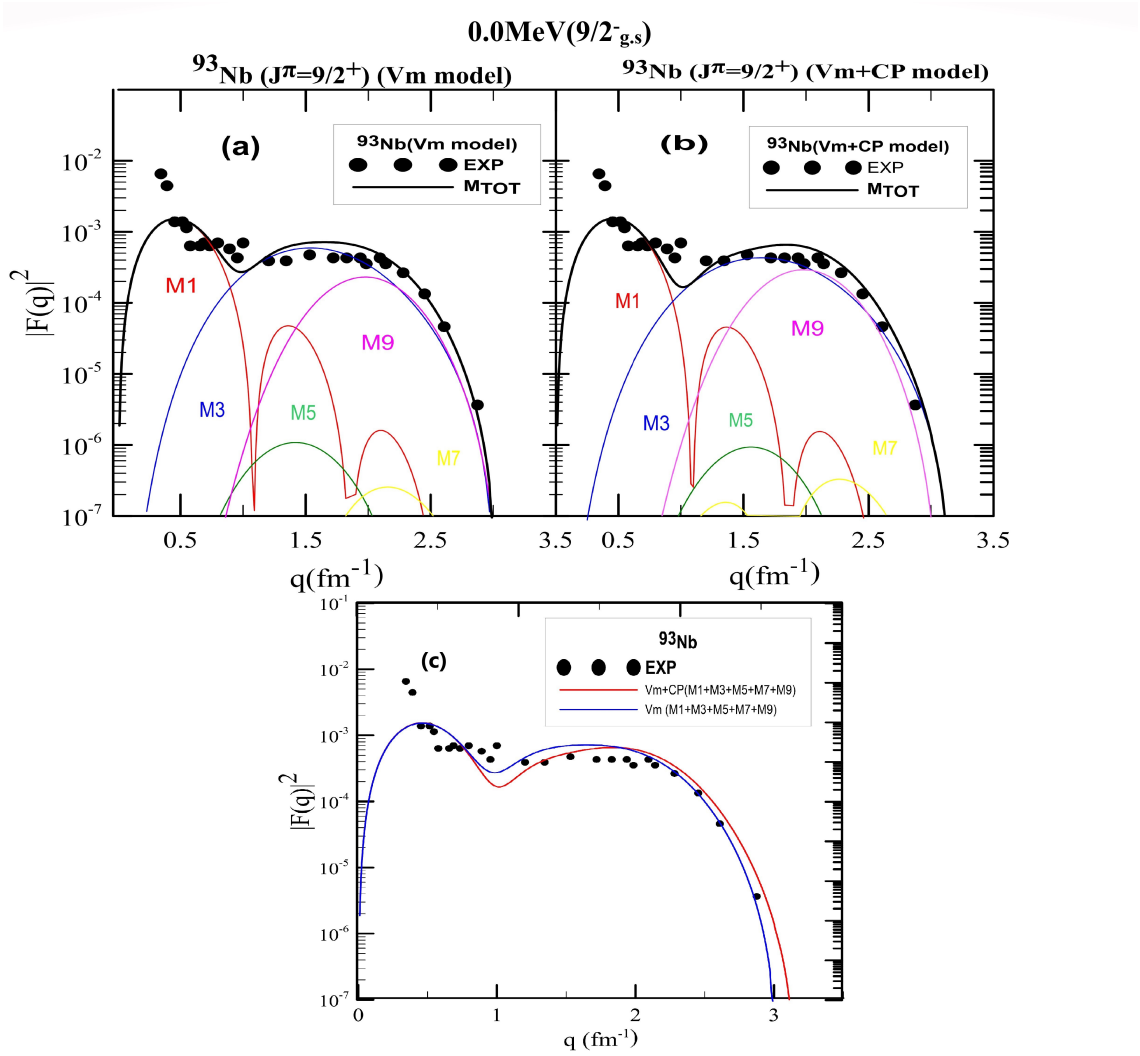

Figure 4.3: The total transverse magnetic form factor for the transition to the $(\frac{9}{2}^{+})$ state in the ^{93}Nb nucleus, without(a),with (b) core-polarization effects and,(c) the relation between momentum transfer q and total magnetic form factor, as it appears with polarization in red and without polarization in blue, respectively. The experimental data are taken from ref. [82, 87, 85].

4.2.4 The nucleus ^{115}In

The transverse form factor calculations have been performed in the (*glekpn* whit restriction) model space since we are interested in the positive-parity states of ^{115}In for the valance particles states (1g 9/2) outside the core ^{56}Ni,The Vm(a) and the Vm with CP model(b) are compared as the total magnetic form factor, which symbolizes the sum. The contribution of M1, M3, M5,M7 and M9 for ^{115}In ($J^{\pi} = \frac{9}{2}^{+}$) is shown in red, blue, green, and yellow, respectively. Effective interaction *glekpn*. It was applied to the g-shell model space wave function. In the first peak between $(0 \leq q \leq 1)fm^{-1}$, the dominant component is M1 where the maximum values are 10^{-3} and $0.5fm^{-1}$ for form factors and momentum transfer values respectively ,At the second peak between $(1.6 \leq q \leq 2.8)fm^{-1}$, the dominant component is M9 where the maximum values is 10^{-4} and $(1.9)fm^{-1}$ for form factors and momentum transfer values respectively.

Figure (4.4) section (c) compares the total magnetic form factor between the Valence model(Vm),shown in blue line ,and the Valence model with core polarization(Vm+Cp), shown in red line. It is clear from the peaks in the figure that the core effect is very small, because the form factor in our work is transverse.

.

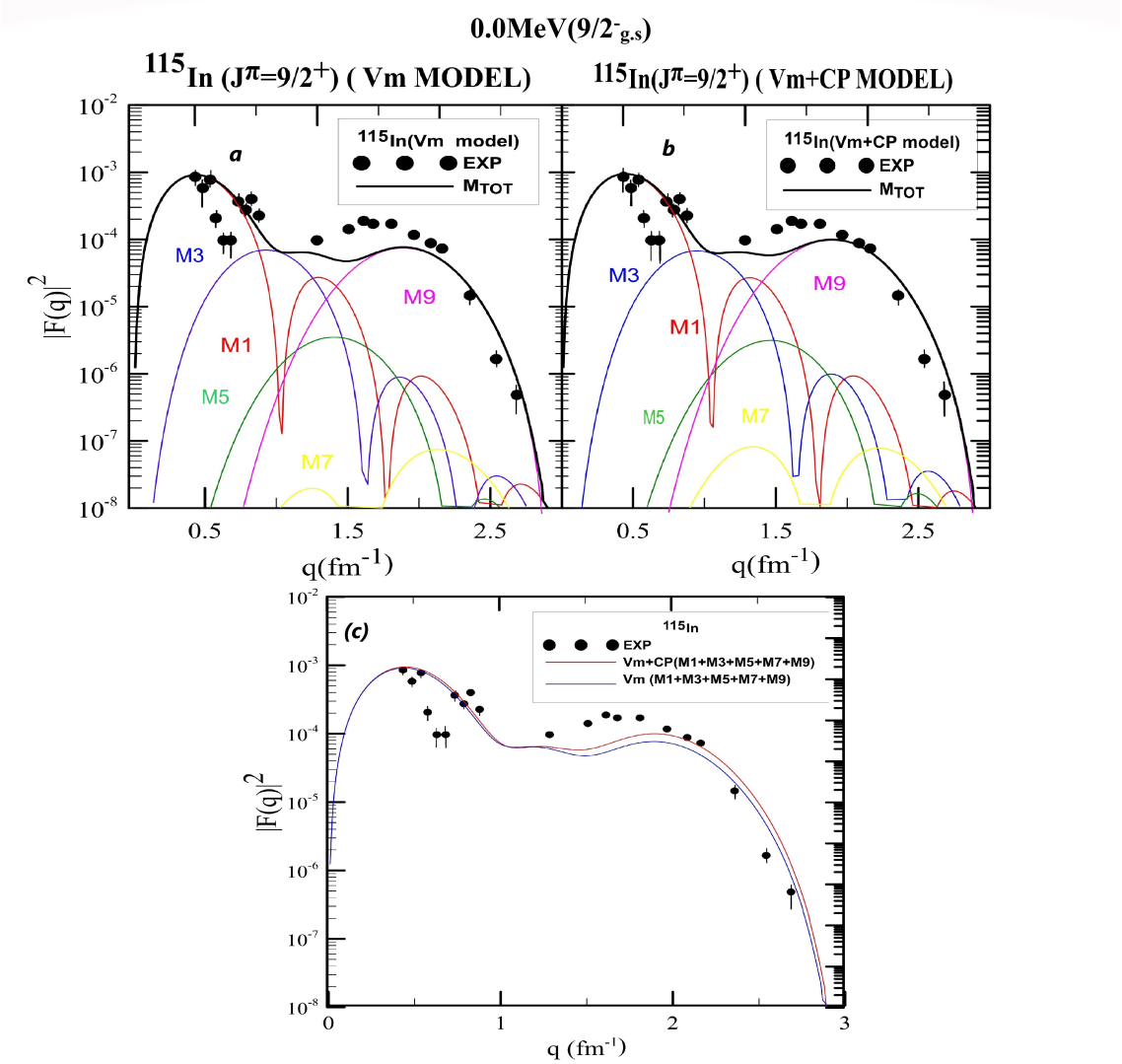

Figure 4.4: The total transverse magnetic form factor for the transition to the $(\frac{9}{2}^{+})$ state in the ^{115}In nucleus, without(a),with (b) core-polarization effects and,(c) the relation between momentum transfer q and total magnetic form factor, as it appears with polarization in red and without polarization in blue, respectively. The experimental data are taken from ref.[82]

4.3 The Longitudinal C2 and C4 Form Factors

4.3.1 The nucleus ^{42}Ca

The nuclear form factor C2 calculation for the ^{42}Ca nucleus using the Tassie(the blue line) and Bohr-Motelsen (the intermittent red) models with core-polarization is shown in Figure (4.5). The calculations were carried out in the region of the model d3f7 by using the effective interaction W0 and using The ^{40}Ca nucleus is closed as the core and thus has ^{42}Ca two nucleons outside the core, where there are two regions for matching the theoretical with the exp. When the nuclear form factor's highest value equals 10^{-4} in the first area $(0 \leq q \leq 1.6), fm^{-1}$, there is a good match. Regarding the second area, there is a near-strong match there and it is situated in the momentum range of $(1.8 \leq q \leq 2.4), fm^{-1}$. Approximately at a nuclear form factor maximum of 10^{-6} .

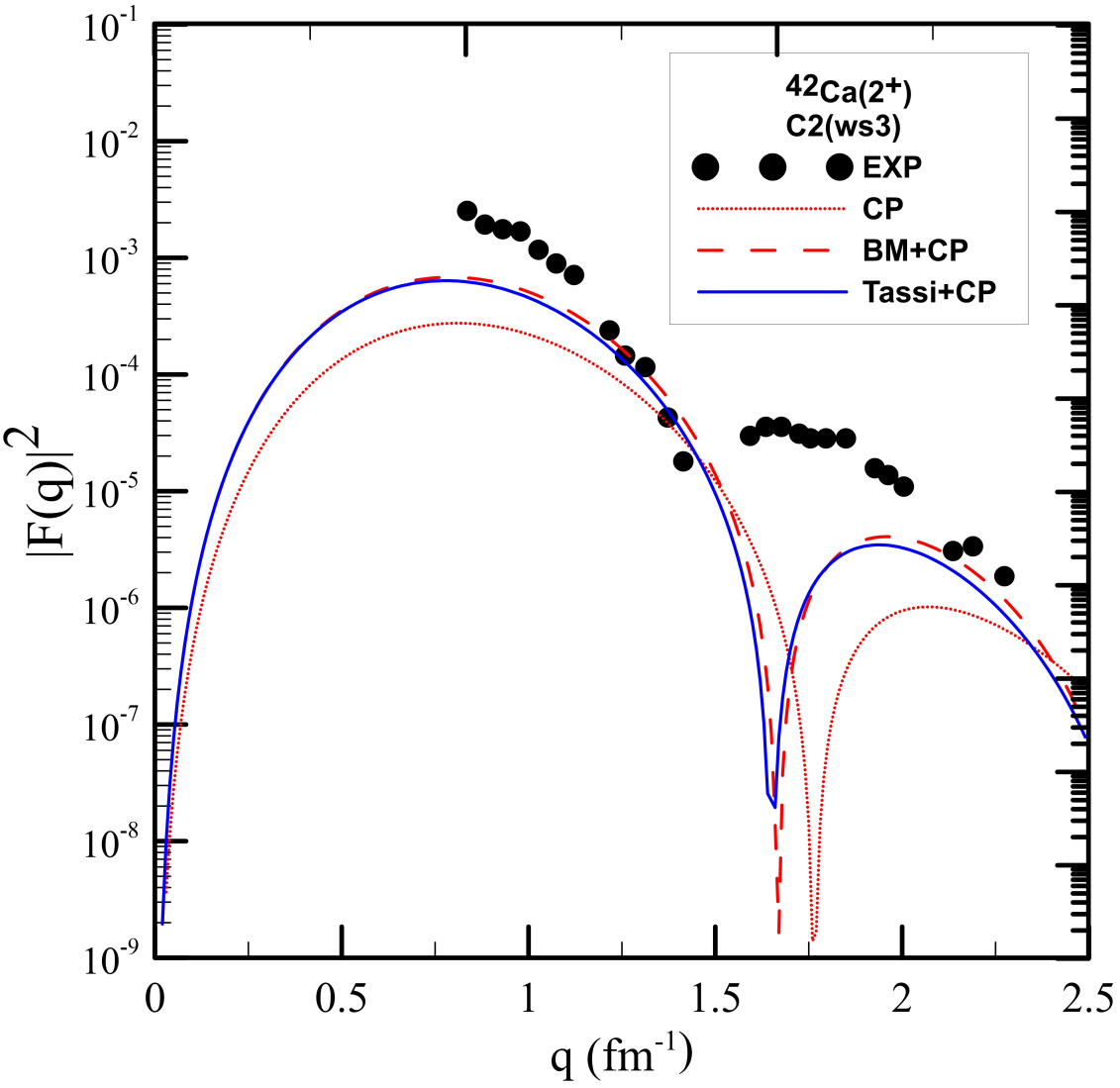

Figure 4.5: The longitudinal form factor C2 in the ^{42}Ca nucleus. The experimental data are taken from ref[88] .

4.3.2 The nucleus ^{44}Ca

The Bohr-Motelsen (The dashed line is red) and Tassie (blue line) models with core-polarization were used to calculate the C2 nuclear form factor of the ^{44}Ca nucleus in Figure (4.6). With a closed core of a ^{40}Ca nucleus and the residual interaction W0, calculations were carried out in the area of the d3f7 pattern, where there are three peaks. When the highest value of the nuclear form factor is 10^{-6} the first peak in the momentum transfer area $(0 \leq q \leq 1.5)$,fm^{-1} has a decent convergence compared to the second peak in the momentum transfer region$(1.5 \leq q \leq 2.5)$, fm^{-1} with 10^{-8} . There is no relationship between the theoretical and the practical for the third peak, which lies between $(2.5 \leq q \leq 3)$,fm^{-1}.

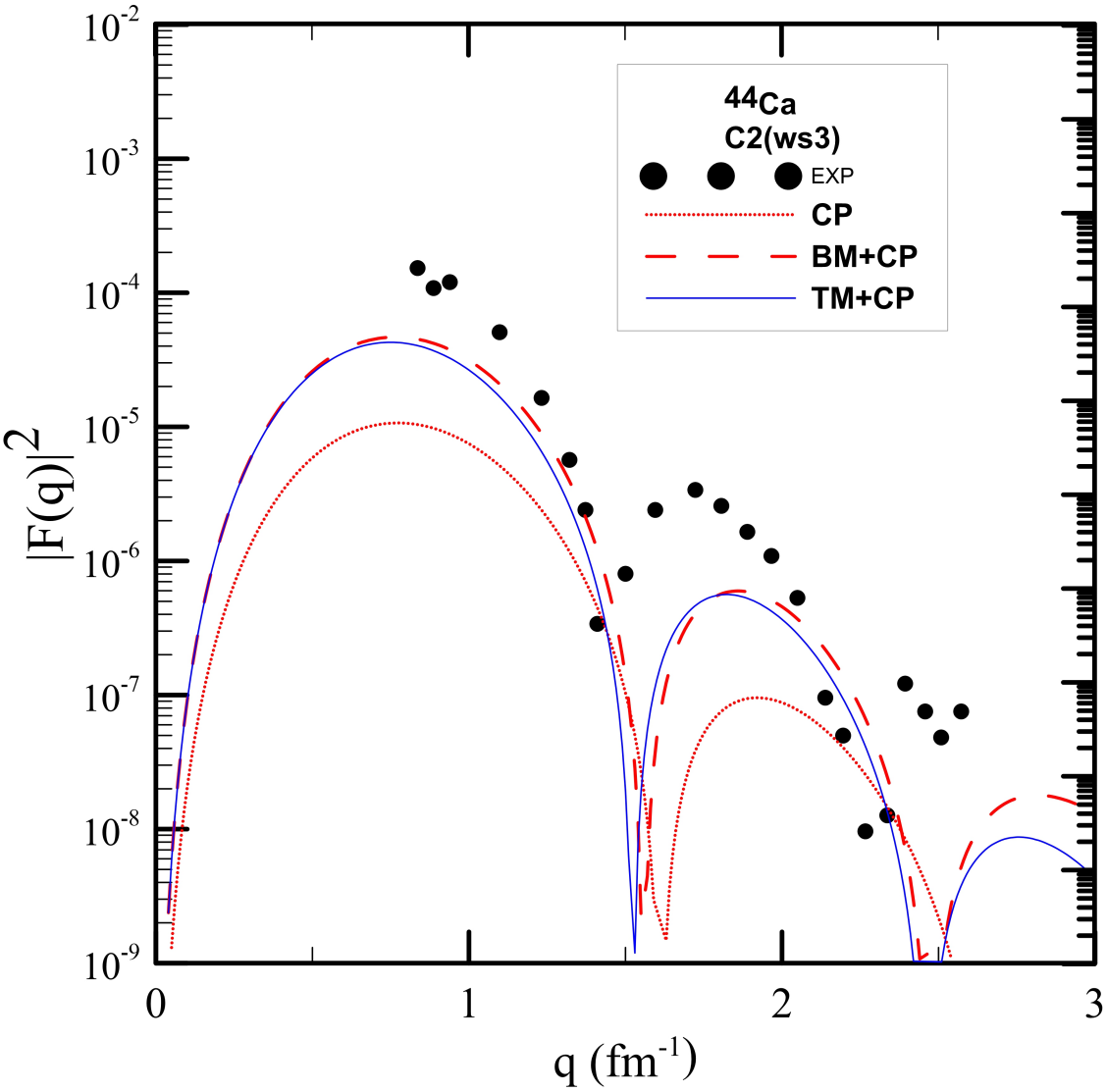

Figure 4.6: The longitudinal form factor C2 in the ^{44}Ca nucleus. The experimental data are taken from ref[88] .

4.3.3 The nucleus ^{48}Ca

The Tassie(blue line) and Bohr-Mottelson (The dashed line is red) models with CP were employed to calculations form factors C2 and C4 of the ^{48}Ca nucleus .The ^{40}Ca core was used as a closed core with 8 particles outside the core^{40}Ca The residual interaction W0, and the potential WS1 and SK35 were used in calculations in the d3f7 model space.

Figure 4.7(a) depicts the data as having two peaks, as indicated in the image below.When the maximum value of the nuclear form factor is 10^{-3}, the first peak in the momentum transfer area $(0 \leq q \leq 1.5)$ fm^{-1} exhibits better convergence than the second peak in the momentum transfer region $(1 \leq q \leq 2.2)$ fm^{-1} with 10^{-5} , since there is no convergence of the theoretical and actual results at this peak.

The longitudinal C4 form factor for the 4^{+} state with the inclusion of the CP effect is plotted in figure 4.7(b) . The results likewise has two peaks, the first peak, which is in the momentum area and has the nuclear form factor $(0.4 \leq q \leq 2.1) fm^{-1}$ with 10^{-5}, exhibits extremely excellent convergence. As for the second peak, there is no correspondence between the exp and the theoretical.

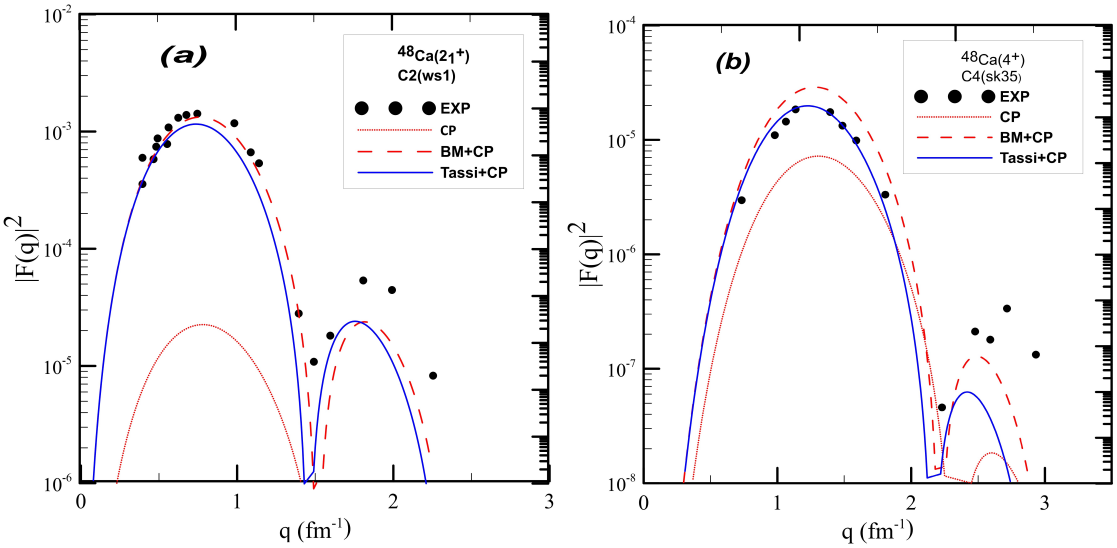

Figure 4.7: The longitudinal form factor C2 and C4 in the ^{48}Ca nucleus. The experimental data are taken from ref[89, 90] .

4.3.4 The nucleus ^{58}Ni

The Tassie(blue line) and Bohr-Mottelson (The dashed line is red) models with CP were employed to calculations form factors C2 and C4 of the ^{58}Ni nucleus .The ^{56}Ni core was used as a closed core with 2 particles outside the core^{56}Ni The residual interaction jj44b, , and the potential WS1 and HO were used in calculations in the jj44 model space.

Figure (4.8) (a), compare the exp. and theoretical longitudinal form factors for ^{58}Ni for the C2 transition. The region of momentum transfer the smaller than 1 fm^{-1} is a good agreement between the experimental date and BM within CP, Tassie within CP, but when the momentum transfer is 1 fm^{-1} the CP is better than BM or Tassie model within CP. In the end of second peak at q= 2 fm^{-1} the BM within CP approximately agreement with the experimental data. The third peak it differs in correspondence between BM and then Tassie models within CP.
In Figure (4.8) (b) the results of C4 form factors for ^{58}Ni nucleus with BM and Tassie model within CP and the jj44b is residual interaction. The calculations of form factor is approximately agreement with experimental data but the CP is better than other when the momentum transfer in region 1.5 fm^{-1}.

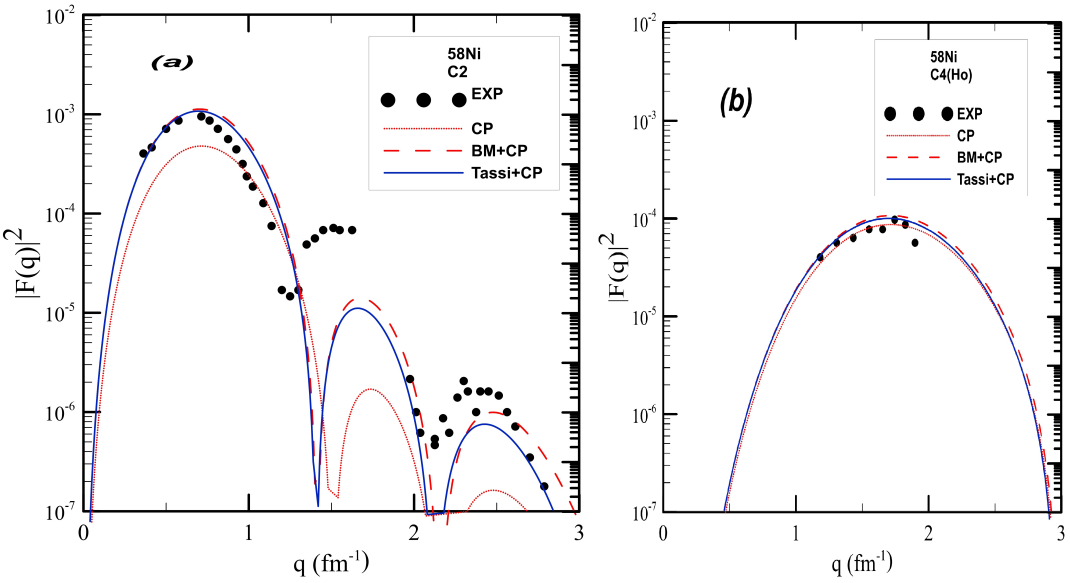

Figure 4.8: The longitudinal form factor C2 and C4 in the ^{58}Ni nucleus. The experimental data are taken from ref[91] .

4.3.5 The nucleus ^{60}Ni

The model space jj44, which includes a core of ^{56}Ni and 4 valence neutrons for ^{60}Ni, was used in the calculations for the shell model.The state longitudinal form factor is C2. ($J^{\pi}T = 2_1^+1$)of ^{60}Ni

In Figure (4.9), the practical results for electron scattering form factor were compared with the theoretical results. The calculations performed with HO as potential and jj44b as residual interaction. We observe three peaks, the first peak occur at $q = 0.7fm^{-1}$ the second at q=1.9 fm^{-1} and the third peak at q=2.6fm^{-1}. All momentum transfer is enhanced by the C2 form factors due to the CP effects, and we see that the findings show excellent agreement with exp. data especially for the first peak up to q=0.8 fm^{-1} with 10^{-3}.

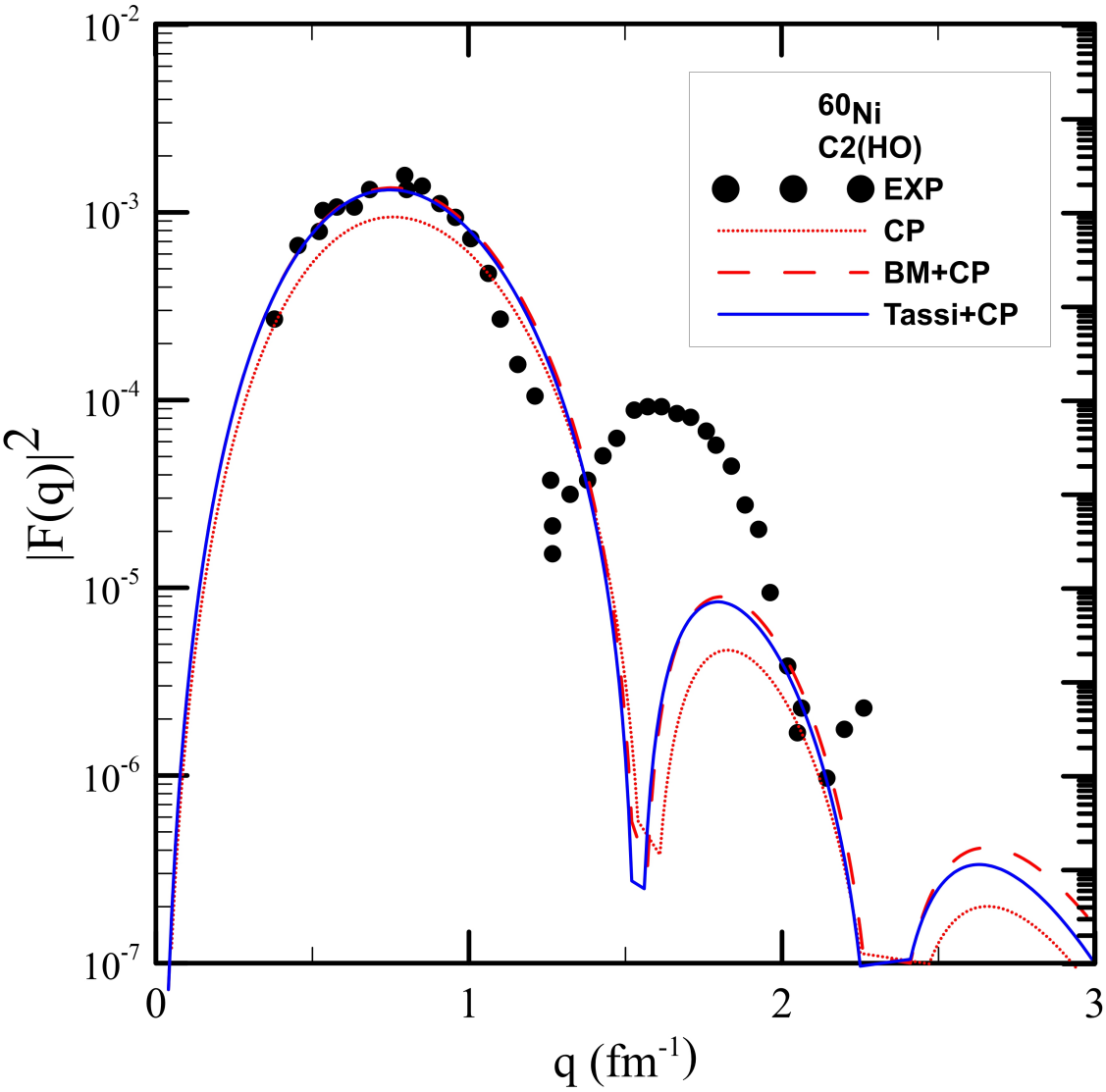

Figure 4.9: The longitudinal form factor C2 in the ^{60}Ni nucleus. The experimental data are taken from ref[91] .

4.3.6 The nucleus ^{62}Ni

The calculations for ^{62}Ni were done using a ^{56}Ni nucleus as a closed core and the residual interaction, jj44b, in the space of the jj44 model. As a result, there are 6 neutrons outside the core ^{56}Ni.

Figure 4.10 (a) shown the C2 form factor for ^{62}Ni nucleus. In the first peak the BM and Tassie models with CP shows better affinities at Momentum transfer is equal to $0.9fm^{-1}$ with 10^{-3} form factor value . But not good agreement in the second and third peak beteewn Theoretical and practical data.

In figure 4.10 (b) has been calculated the C4 form factor for ^{62}Ni nucleus and the calculation of Tassie model(blue line) with CP is closest to practical results in end of first peak. In the second peak the result is not good agreement with the exp. .

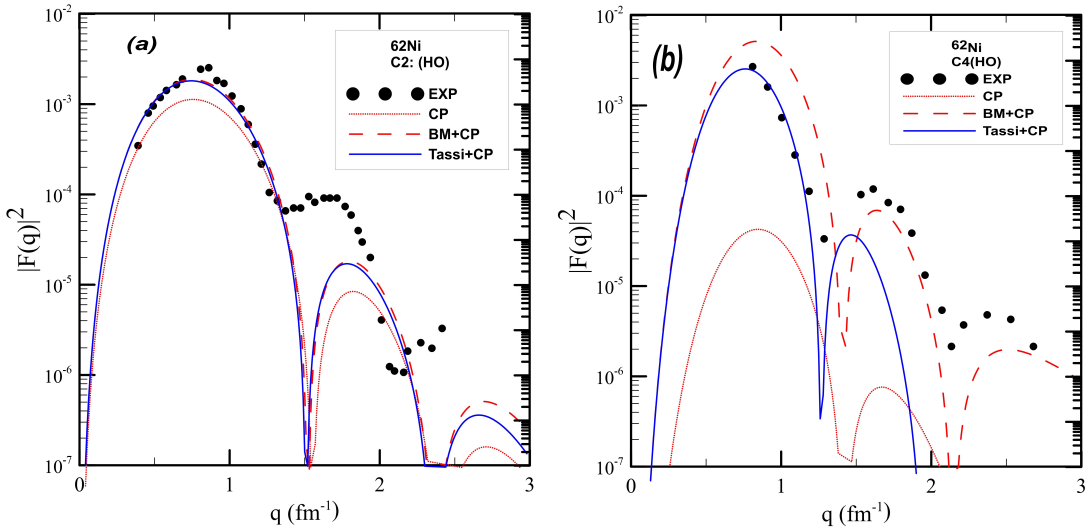

Figure 4.10: The longitudinal form factor C2 and,C4 in the ^{62}Ni nucleus. The experimental data are taken from ref[91] .

4.4 Conclusions

The present study focused on using Tassie and Bohr-Mottelson models to calculate the inelastic electron scattering form factors for some selected states of fp-shell nuclei,therfore we had concluded the following;

1. The transverse magnetic form factors are not sensitive to the change of the effective charge and are well reproduced by both Tassie and Boh-Mottelson models.

2. The harmonic oscillator (HO) is an adequate choice as residual effective interaction for the form factors calculations with specific effective proton and neutron effective charges.

3. The core polarization by means of effective charges of proton and neutron is able to reproduce the form factors for all the studied states of the selected nuclei understudy.

4.5 Suggestions of Future Work

We suggest the following:

1. Extending this work in an attempt using some other residual effective interaction such a slgm, slgtpn, and snt.

2. Extending this work in an attempt to include the other nuclei in the W0, ho, glekpn, and jj44b.

References

References

[1] Samuel SM Wong. Introductory nuclear physics. John Wiley & Sons, 1998

[2] Maria Goeppert Mayer. “On closed shells in nuclei. II”. In: Physical Review 75.12 (1949), p. 1969.

[3] Otto Haxel, J Hans D Jensen, and Hans E Suess. “On the” magic numbers” in nuclear structure”. In: Physical Review 75.11 (1949), p. 1766

[4] MP Fewell. “The atomic nuclide with the highest mean binding energy”. In: American Journal of Physics 63.7 (1995), pp. 653–658

[5] B Alex Brown. “The nuclear shell model towards the drip lines”.In: Progress in Particle and Nuclear Physics 47.2 (2001), pp. 517–599

[6] Yutaka Utsuno . “Varying shell gap and deformation in N 20unstable nuclei studied by the Monte Carlo shell model”. In: Physical Review C 60.5 (1999), p. 054315.

[7] L Coraggio . “Effective shell-model hamiltonians from realistic nucleon–nucleon potentials within a perturbative approach”. In: Annals of Physics 327.9 (2012), pp. 2125–2151.

[8] Kenneth S Krane. Introductory nuclear physics. John Wiley & Sons, 1991.

[9] Radha Raman Roy and Bishan P Nigam. Nuclear physics: theory and experiment. Wiley, 1967.

[10] JD Walecka. “Electron scattering”. In: Nuclear Physics, A;(Netherlands) 574 (1994).

[11] T de Forest Jr and John Dirk Walecka. “Electron scattering and nuclear structure”. In: Advances in Physics 15.57 (1966), pp. 1–109.

[12] Nevill Francis Mott. “The scattering of fast electrons by atomic nuclei”. In: Proceedings of the Royal Society of London. Series A, Containing Papers of a Mathematical and Physical Character 124.794 (1929), pp. 425–442.

[13] A St J Murphy . “Level structure of Mg 21: Nuclear and astrophysical implications”. In: Physical Review C 73.3 (2006),p. 034320.

[14] M Honma . “Effective interaction for pf-shell nuclei”. In: Physical Review C 65.6 (2002), p. 061301.

[15] D Zwarts. “RITSSCHIL, a new program for shell-model calculations”. In: Computer Physics Communications 38.3 (1985), pp. 365–388

[16] Etienne Caurier . “The shell model as a unified view of nuclear structure”. In: Reviews of modern Physics 77.2 (2005), p. 427.

[17] A Schmidt . “Low spin structure of the N= Z odd-odd nucleus 25 50 Mn 25”. In: Physical Review C 62.4 (2000), p. 044319.

[18] BA Brown and WDM Rae. “The shell-model code NuShellX@ MSU”. In: Nuclear Data Sheets 120 (2014), pp. 115–118.

[19] Stephan Narison. QCD as a theory of hadrons: from partons to confinement. Vol. 17. Cambridge University Press, 2004

[20] Igal Talmi. Simple models of complex nuclei. Routledge, 2017

[21] Aage Bohr and Ben R Mottelson. “Rotational states in even-even nuclei”. In: Physical Review 90.4 (1953), p. 717

[22] F Petrovich . “Core polarization in inelastic scattering”. In: Physical Review C 16.2 (1977), p. 839.

[23] Aage Niels Bohr and Ben R Mottelson. Nuclear Structure (in 2 volumes). World Scientific Publishing Company, 1998

[24] B Alex Brown, Raad Radhi, and Bryan Hobson Wildenthal. “Electric quadrupole and hexadecupole nuclear excitations from the perspectives of electron scattering and modern shell-model theory”. In: Physics Reports 101.5 (1983), pp. 313–358.57

[25] Khalid S Jassim and Shamil R Sahib. “Large-scale shell model calculations of the ^{25,} ^{26}Mg, ^{27}Al and ^{19}F nucleus”. In: International Journal of Nuclear Energy Science and Technology 12.1 (2018), pp. 81–91.

[26] Khalid S Jassim. “The electron scattering form factor of ^{10}B, ^{32}S and ^{48}Ca nuclei”. In: Physica Scripta 86.3 (2012), p. 035202

[27] Khalid S Jassim and HA Kassim. "Core Polarization Effects of some odd sd-shell nuclei using M3Y effective nucleon-nucleon interaction". In: Romanian Journal of Physics 58.3-4 (2013), pp. 319–29

[28] Adie D Salman, Nadia M Adeeb, and Mohannad H Oleiwi."Core-polarization effects on the inelastic longitudinal C2 and C4 form factors of $^{46, 48, 50}$ Ti nuclei". In: Journal of Nuclear and Particle Physics 3.1 (2013), pp. 20–24.

[29] Khalid S Jassim ."Elastic and inelastic electron-nucleus scattering form factors of some light nuclei: ^{23}Na, ^{25}Mg, ^{27}Al , and^{41} Ca ". In: Physical Review C 89.1 (2014),

p. 014304

[30] Khalid S Jassim and Zahraa M Abdul-Hamza. "LONGITUDINAL (C2) FORM FACTORS WITH CORE-POLARIZATION EFFECTS OF SOME FP-SHELL NUCLEI USING TASSIE MODEL." In: Armenian Journal of Physics 7.4 (2014).

[31] James M Allmond . "High-precision B (E 2) measurements of semi-magic ^{58,60,62,64}Ni by Coulomb excitation".In: Physical Review C 90.3 (2014), p. 034309

[32] Anwer A Al-Sammarraie . "Longitudinal and transverse electron-nucleus scattering form factors of ^{25} Mg ". In: Physical Review C 92.3 (2015), p. 034327

[33] Mohanad Hussein Oleiwi and Khalid S Jassim. "Core Polarization Effects on the Inelastic Longitudinal C2 and C4 Form Factors of $^{58, 60, 62}$ Ni Nuclei". In: Journal of University of Babylon 24.5(2016).

[34] Khalid S Jassim and Aqeel I Faris. "Nuclear structure of ^{60}Ni nucleus using shell model calculations". In: Journal of Computational and Theoretical Nanoscience 14.5 (2017), pp. 2336–2340

[35] Ali A Alzubadi. "Transverse Magnetic Electron Scattering Form Factors for Some Odd-A Nuclei Using Shell Model and Hartree–Fock Calculations". In: Iranian Journal of Science and Technology, Transactions A: Science 42 (2018), pp. 2387–2396.

[36] Pedro Sarriguren . "Elastic magnetic electron scattering from deformed nuclei". In: Physical Review C 99.3 (2019), p. 034325

[37] Adie D Salman, Samah A Al-Ramahi, and MH Oleiwi. “Inelastic electron-nucleus scattering form factors for $^{64, 66, 68}$Zn isotopes”. In: AIP Conference Proceedings. Vol. 2144. 1. AIP Publishing LLC. 2019, p. 030029.

[38] Sara J Ahmad, Khalid S Jassim, and Fouad A Majeed. “The effect of core polarization by means of Tassie and Bohr-mottelson models for some FP-shell nuclei”. In: Jour of Adv Research in Dynamical & Control Systems 12.5 (2020).

[39] Doaa Murshedi and AD Salman. “Estimation of Inelastic Longitudinal Electron Scattering Form Factors in $^{58, 60}$Ni Nuclei Using OXBASH Code”. In: Journal of Nuclear Sciences 7.1 (2021),pp. 1–8.

[40] Khalid S Jassim and Ranya Mahmoud Mohammed. “Coulomb Form Factors of ^{27} Al and ^{31}P Nuclei Using Coulomb valance Tassie model and Bohr-Mottelson Collective Models with Different Potentials”. In: arXiv preprint arXiv:2207.13804 (2022).

[41] Nawres T. Sheehab and Fouad A. Majeed “Form Factor and Charge Density Distribution Calculations for ^{58}Ni, ^{70,72}Ge Isotopes by Using Skyrme Interaction in NushellX@MSU Code” .In: Neuro Quantology . Vol. 20(5): (2022), pp. 368-373

[42] Sarah M Obaid and Fouad A Majeed. “Longitudinal and transverse form factors from ^{65}Cu and ^{71}Ga nuclei”. In: Journal of the Korean Physical Society 82.4 (2023), pp. 329–339.

[43] Ali Abdulateef Alzubadi and GW Harby. “Calculation of the electromagnetic moments and electroexcitation form factors for some boron isotopes using shell model with skyrme interaction”. In: Revista Mexicana de Fısica 69.1 Jan-Feb (2023), pp. 011202–1.

[44] A Bodek and ME Christy. “Contribution of Nuclear Excitation Electromagnetic Form Factors in {rm ^{12} C} and {\rm^{16} O}to the Coulomb Sum Rule” . In: arXivm preprint arXiv:2301.05650 (2023).

[45] PJ Brussaard and PWM Glademans. Shell-model Application in “Nuclear Spectroscopy” North. 1977.

[46] John Dirk Walecka. Theoretical nuclear and subnuclear physics. World Scientific, 2004.

[47] PJ Brussaard . “Theory, ch. 4”. In: (1977).

[48] Lynne C Remer and Jan H Jensen. “Toward a General Theory of Hydrogen Bonding: The Short, Strong Hydrogen Bond [HOH OH]-”. In: The Journal of Physical Chemistry A 104.40 (2000), pp. 9266–9275.

[49] K Langanke . “Shell-model Monte Carlo studies of fp-shell nuclei”. In: Physical Review C 52.2 (1995), p. 718.

[50] Nathan Hoteling. “Structure of iron isotopes at the limits of the p-f shell”. PhD thesis. University of Maryland, College Park, 2008.

[51] John Markus Blatt and Victor Frederick Weisskopf. Theoretical nuclear physics. Courier Corporation, 1991.

[52] B Alex Brown. “Lecture notes in nuclear structure physics”. In: National Super Conducting Cyclotron Laboratory 11 (2005).

[53] Tomas Dytrych . “Efficacy of the SU (3) scheme for ab initio large-scale calculations beyond the lightest nuclei”. In: Computer Physics Communications 207 (2016), pp. 202–210.

[54] RA Radhi and EA Salman. “Collective E2 transitions in ^{18}O”. In: Nuclear Physics A 806.1-4 (2008), pp. 179–190.

[55] M Fabre de la Ripelle, SA Sofianos, and RM Adam. “Method for solving the many-body bound state nuclear problem”. In: Annals of Physics 316.1 (2005), pp. 107–159.

[56] Carl B Dover and Nguyen Van Giai. “The nucleon-nucleus potential in the Hartree-Fock approximation with Skyrme’s interaction”. In: Nuclear Physics A 190.2 (1972), pp. 373–400.

[57] Roger D Woods and David S Saxon. “Diffuse surface optical model for nucleon-nuclei scattering”. In: Physical Review 95.2 (1954),p. 577.

[58] THR Skyrme. “The effective nuclear potential”. In: Nuclear Physics 9.4 (1958), pp. 615–634.

[59] Ruprecht Machleidt. “Computational Nuclear Physics 2–Nuclear Reactions”. In: Langanke, Maruhn, Koonin, eds., Springer NY (1993), p. 1.

[60] Jenny Lee . “Neutron spectroscopic factors of ^{34}Ar and ^{46}Ar from (p, d) transfer reactions”. In: Physical Review C 83.1 (2011), p. 014606.

[61] Walter Greiner, Joachim A Maruhn, . Nuclear models. Springer, 1996.

[62] L J Tassie. “A model of nuclear shape oscillations for g? Transitions and electron excitation”. In: Australian Journal of physics 9.4 (1956), pp. 407–418.

[63] James Rainwater. “Nuclear energy level argument for a spheroidal nuclear model”. In: Physical Review 79.3 (1950), p. 432.

[64] A Bohr . “Nuclear structure, vol. 2: Nuclear deformations”. In: Physics Today 30.3 (1977), p. 59.

[65] David Lawrence Hill and John Archibald Wheeler. “Nuclear constitution and the interpretation of fission phenomena”. In: Physical Review 89.5 (1953), p. 1102.

[66] Judah M Eisenberg and Walter Greiner. “Nuclear theory”. In: (1987).

[67] L Pŕ ochniak and SG Rohozĭ nski. “Quadrupole collective states within the Bohr collective Hamiltonian”. In: Journal of Physics G: Nuclear and Particle Physics 36.12 (2009), p. 123101.

[68] G Gneuss, U Mosel, and W Greiner. “A new treatment of the collective nuclear Hamiltonian”. In: Physics Letters B 30.6 (1969), pp. 397–399

[69] Ben Mottelson. “Elementary modes of excitation in the nucleus”. In: Reviews of Modern Physics 48.3 (1976), p. 375.

[70] Herbert Uberall. “Electron Scattering From Complex Nuclei ’’V36A. Academic Press, 2012.

[71] T William Donnelly and JD Walecka. “Electron scattering and nuclear structure”. In: Annual Review of Nuclear Science 25.1 (1975), pp. 329–405.

[72] Amos DeShalit and Herman Feshbach. “Theoretical nuclear physics. Volume I. Nuclear structure”. In: (1974).

[73] PJ Brussaard and PWM Glaudemans: “Shell-Model Applications in Nuclear Spectroscopy ’’ , North-Holland, Amsterdam and New York, 1977, xii+ 452 , 23× 16cm, 22,400 . In: 34.6 (1979), pp. 525–526.

[74] T-SH Lee and D Kurath. “Inelastic pion scattering for 1 p-shell targets”. In: Physical Review C 21.1 (1980), p. 293.

[75] K Kaneko . “Structure of upper-g 9/2-shell nuclei and shape effect in the Ag 94 isomeric states”. In: Physical Review C 77.6 (2008), p. 064304.

[76] L Jo Tassie and FC Barker. “Application to electron scattering of center-of-mass effects in the nuclear shell model”. In: Physical Review 111.3 (1958), p. 940.

[77] TW Donnelly and JD Walecka. “Elastic magnetic electron scattering and nuclear moments”. In: Nuclear Physics A 201.1 (1973), pp. 81–106.

[78] WK Koo and LJ Tassie. “Electron excitations and sum rules for multi-pole transitions”. In: Australian Journal of Physics, vol. 34, p. 15 34 (1981), p. 15.

[79] AN Antonov, PE Hodgson, and I Zh Petkov. Nucleon Momentum and Density Distributions in Nuclei Clarendon. 1988.

[80] AN Antonov . “Generator coordinate calculations of nucleon momentum and density distributions in ^{4}He, ^{16}O and ^{40}Ca”. In: Il Nuovo Cimento A (1965-1970) 100.5 (1988), pp. 779–788.

[81] J Friedrich and P-G Reinhard. “Skyrme-force parametrization: Leastsquares fit to nuclear ground-state properties”. In: Physical Review C 33.1 (1986), p. 335.

[82] T William Donnelly and Ingo Sick. “Elastic magnetic electron scattering from nuclei”. In: Reviews of modern physics 56.3 (1984), p. 461.

[83] K Arita . “Magnetization distribution of ^{51}V studied by elastic electron scattering through 180°”. In: Physical Review C 23.4 (1981), p. 1482.

[84] SK Platchkov . “The magnetic form factor of ^{51}V at very high momentum transfer”. In: Physics Letters B 131.4-6 (1983), pp. 301–304.

[85] SK Platchkov . “Magnetic electron scattering and valence nucleon radial wave functions”. In: Physical Review C 25.5 (1982), p. 2318.

[86] H De Vries, GJC Van Niftrik, and L Lapikas. “Elastic electron scattering through 180° from the magnetization distribution of the 1f72-shell nuclei Sc, V and Co”. In: Physics Letters B 33.6 (1970), pp. 403–406.

[87] RC York and GA Peterson. “180° elastic electron scattering from the magnetization distributions of ^{25}Mg and ^{93}Nb”. In: Physical Review C 19.3 (1979), p. 574.

[88] J Heisenberg, JS McCarthy, and I Sick. “Inelastic electron scattering from several Ca, Ti and Fe isotopes”. In: Nuclear Physics A 164.2 (1971), pp. 353–366.

[89] Paul Buck Mast. “STYLE AND STRUCTURE IN IBERIA” BY ISAAC ALBENIZ. University of Rochester, Eastman School of Music, 1974.

[90] JE Wise et al. “Inelastic electron scattering from ^{48}Ca ”. In: Physical Review C 31.5 (1985), p. 1699.

[91] H De Vries, CW De Jager, and C De Vries. “Nuclear charge density-distribution parameters from elastic electron scattering”. In: Atomic data and nuclear data tables 36.3 (1987), pp. 495–536.

الخلاصة

تمت دراسة عوامل التشكل العرضية للأستطارة الإلكترونية لبعض الحالات المختارة من النوى ^{51}V, ^{59}Co, ^{93}Nb, ^{115}In مع عوامل التشكل الطولية للأستطارة الإلكترونية لبعض الحالات المختارة من النوى $^{58,60,62}Ni$, $^{40,42,44,48}Ca$ حيث تقع في منطقة fp. تم إجراء حسابات أنموذج القشرة باستخدام الإصدار الأخير من البرنامج الحاسوبي NushellX @ MSU.

تم أستخدام التفاعلات المؤثرة في النوى لحساب القيمة الذاتية والمتجهات الذاتية المستخدمة لحساب كثافات انتقال الجسم الواحد (OBTD) لاستخدامها في حسابات عوامل شكل تشتت الإلكترون غير المرن.

تم استخدام نماذج Tassie و Bohr-Mottelson لحساب عوامل التشكل النووي للأستطارة الإلكترونية غير المرنة باستخدام مذبذب توافقي (HO) كتفاعل فعال متبقي. تُستخدم الشحنات الفعالة للبروتون والنيوترون لحساب تأثيرات أستقطاب القلب.

يتم استخدام تفاعل Skyrme الفعال مع معاملات (Sk35) في حساب عوامل التشكل باستخدام دالة موجة الفضاء النموذجية الناتجة عن تداخل جميع الدوال الموجة الناتجة عند خلط جميع حالات فضاء الأنموذج المعتمدة دون أي القيود المفروضة على فضاء الأنموذج.

تمت مقارنة عوامل التشكل للأستطارة الإلكترونية غير المرنة المحسوبة للنواة المدروسة مع البيانات التجريبية المتوفرة. تم الوصول الى أن تأثير أستقطاب القلب عن طريق الشحنات الفعالة للبروتونات والنيوترونات أمرًا ضروريًا للغاية ليتم أخذه في الاعتبار والذي يحسن التوافق مع البيانات التجريبية جيدًا ، خاصة بالنسبة لعوامل التشكل الكولومية C2 و C4. تتأثر عوامل الشكل المغناطيسي بدرجة أقل أو لا تتأثر بتغير شحنة البروتون والنيوترون الفعالة.

جمهورية العراق
وزارة التعليم العالي و البحث العلمي
جامعة بابل
كلية التربية للعلوم الصرفة
قسم الفيزياء

دراسة تأثير استقطاب القلب باستخدام حسابات انموذج القشرة المجهري في بعض النوى

رسالة مقدمة الى مجلس كلية التربية للعلوم الصرفة في جامعة بابل و هي جزء من متطلبات نيل درجة الماجستير في التربية / الفيزياء

قدمها الطالب

سجاد علي خشان ماضي

(بكالوريوس فيزياء/ جامعة بابل 2018 م)

بأشراف

أ. د. خالد صالح جاسم الجُميلي

1445 هـ **2023 م**